Quaternary Research 83 (2015) 378–393

Contents lists available at ScienceDirect

Quaternary Research

journal homepage: www.elsevier.com/locate/yqres

Quaternary tephrochronology and deposition in the subsurface Sacramento–San Joaquin Delta, California, U.S.A.

Katherine L. Maier [a,*], Emma Gatti [a,b], Elmira Wan [c], Daniel J. Ponti [a], Mark Pagenkopp [d], Scott W. Starratt [e], Holly A. Olson [c], John C. Tinsley [a]

[a] U.S. Geological Survey, Earthquake Science Center, 345 Middlefield Road Mail Stop 977, Menlo Park, CA 94025, USA
[b] Planetary Surface Instruments Group, NASA Jet Propulsion Laboratory, California Institute of Technology, 4800 Oak Grove Drive, Pasadena, CA 91109, USA
[c] U.S. Geological Survey, Geology, Minerals, Energy, and Geophysics Science Center, 345 Middlefield Road Mail Stop 975, Menlo Park, CA 94025, USA
[d] California Department of Water Resources, 3500 Industrial Boulevard, West Sacramento, CA 95691, USA
[e] U.S. Geological Survey, Volcano Science Center, 345 Middlefield Road Mail Stop 910, Menlo Park, CA 94025, USA

ARTICLE INFO

Article history:
Received 5 March 2014
Available online 7 February 2015

Keywords:
Tephra
Volcanic ash
Pumice
Facies
Rockland ash bed
Loleta ash bed
Sacramento–San Joaquin Delta
Cascades
Fluvial channel
Chronostratigraphy

ABSTRACT

We document characteristics of tephra, including facies and geochemistry, from 27 subsurface sites in the Sacramento–San Joaquin Delta, California, to obtain stratigraphic constraints in a complex setting. Analyzed tephra deposits correlate with: 1) an unnamed tephra from the Carlotta Formation near Ferndale, California, herein informally named the ash of Wildcat Grade (<~1.450 to >~0.780 Ma), 2) the Rockland ash bed (~0.575 Ma), 3) the Loleta ash bed (~0.390 Ma), and 4) middle Pleistocene volcanic ash deposits at Tulelake, California, and Pringle Falls, Bend, and Summer Lake, Oregon, herein informally named the dacitic ash of Hood (<~0.211 to >~0.180 Ma). All four tephra are derived from Cascades volcanic sources. The Rockland ash bed erupted from the southern Cascades and occurs in up to >7-m-thick deposits in cores from ~40 m subsurface in the Sacramento–San Joaquin Delta. Tephra facies and tephra age constraints suggest rapid tephra deposition within fluvial channel and overbank settings, likely related to flood events shortly following volcanic eruption. Such rapidly deposited tephra are important chronostratigraphic markers that suggest varying sediment accumulation rates in Quaternary deposits below the modern Sacramento–San Joaquin Delta. This study provides the first steps in a subsurface Quaternary stratigraphic framework necessary for future hazard assessment.

Published by Elsevier Inc. on behalf of University of Washington.

Introduction

Tephra deposits (including volcanic ash, pumice clasts, lapilli, and glass shards) are important correlation tools that can be used to constrain time surfaces in sedimentary successions (e.g., Sarna-Wojcicki, 2000; Lowe, 2008, 2011; Nooren et al., 2009; Addison et al., 2010; Salisbury et al., 2012). Additionally, detailed description and interpretation of tephra deposits including facies analysis can lead to a better understanding of depositional processes (e.g., Nakayama and Yoshikawa, 1997; Kataoka, 2005; Kataoka et al., 2009; Manville et al., 2009; Lowe, 2011; Gatti et al., 2011, 2013; Tripaldi et al., 2011). In this study, analysis and correlation of identified tephra deposits aid subsurface chronostratigraphic correlations and depositional environment interpretations in the complex setting of the Sacramento–San Joaquin Delta (also referred to herein as the delta), California, an important area for natural hazards, freshwater supply, ecosystems, tectonics, and sediment transport and deposition.

The Sacramento–San Joaquin Delta includes the lower reaches of the Sacramento and San Joaquin rivers and the confluence of these two rivers upstream from San Francisco Bay (Fig. 1). Rivers presently drain the interior of central and northern California into the delta (~1400 km^2) and create a region of wetlands that have been anthropogenically modified into agricultural lands beginning in the mid-19th century (Jackson and Paterson, 1977; Logan, 1990; Ingebritsen et al., 2000). The modern Sacramento–San Joaquin Delta is dominated by peat deposits, developed during the Holocene, and intervening fluvial channels (e.g., Drexler et al., 2009, 2014). Agricultural development and farming of peat soils have led to oxidation and compaction of peat soils and subsidence of the region below sea level (Deverel and Rojstaczer, 1996; Ingebritsen et al., 2000; Mount and Twiss, 2005; Coons et al., 2008). Levees and a complex system of waterways have been constructed to keep saline sea water out of the delta, protect shipping lanes, prevent destructive flooding of the islands, and maintain California's freshwater supplies (Jackson and Paterson, 1977; Ingebritsen et al., 2000; Burton and Cutter, 2008). Only the westernmost modern Sacramento–San Joaquin Delta experiences brackish water conditions, and this has been consistent into the Pleistocene and throughout the Holocene (Byrne et al., 2001; Starratt 2002, 2004; Drexler et al., 2014). During Pleistocene climatic fluctuations, the Sacramento–San Joaquin Bay-Delta encompassed fluvial systems, with the modern drainage configuration being established by ~0.6–0.4 Ma (Barnard et al., 2013 and references therein).

* Corresponding author at: U.S. Geological Survey, Pacific Coastal and Marine Science Center, 400 Natural Bridges Drive, Santa Cruz, CA 95060, USA.
E-mail address: kcoble@usgs.gov (K.L. Maier).

http://dx.doi.org/10.1016/j.yqres.2014.12.007
0033-5894/Published by Elsevier Inc. on behalf of University of Washington.

The modern Sacramento–San Joaquin Delta (Fig. 1) is the epicenter of numerous risk assessment, land management, water resource, infrastructure, and agricultural issues (e.g., Ingebritsen et al., 2000) because the fresh water supply for >2/3 of California moves through the delta waterways. The delta contains abundant agriculture, diverse wetland ecosystems, and growing urban areas. Levees within the delta, and the populations, infrastructure, freshwater, and agriculture behind them, are potentially at risk of failure related to shaking and liquefaction during an earthquake (Finch, 1988; Wong et al., 2006; Burton and Cutter, 2008; Real and Knudsen, 2009; Real et al., 2010). Seismic activity is possible along numerous faults in the adjacent San Francisco Bay area, where several large-magnitude (>*M*6.0) earthquakes have occurred in historic times (e.g., Yu and Segall, 1996; Unruh and Krug, 2007; Unruh et al., 2009). Chronostratigraphic markers, such as tephra layers, are critically important for calibrating Quaternary stratigraphic relationships necessary to address seismic and liquefaction hazard assessment, infrastructure planning, and water management in the delta.

Existing documentation and interpretation of deposits in and below the modern Sacramento–San Joaquin Delta are focused on surficial exposures and shallow boreholes (<15 m) (e.g., Atwater, 1982; Goman and Wells, 2000; Brown and Pasternack, 2004; Drexler et al., 2014). In particular, studies have addressed the increased subsidence in delta islands with respect to reclamation, agriculture, peat soils, and wetland ecosystems (e.g., Deverel and Rojstaczer, 1996; Jassby and Cloern, 2000; Drexler et al., 2007), and detailed chronology of small regions has focused on the Holocene (e.g., Ingram et al., 1996; Goman and Wells, 2000; Byrne et al., 2001; Starratt, 2002, 2004; Brown and Pasternack, 2004; Wright and Schoellhamer, 2005; Drexler et al., 2014). Although a geologic context for the Quaternary of the region has been established from surface mapping (e.g., Atwater, 1982; Lettis, 1982), additional subsurface chronostratigraphic markers are needed to extend Quaternary stratigraphic framework into deposits buried below the modern Sacramento–San Joaquin Delta. Buried Pleistocene and Holocene deposits contain material properties that will direct ongoing infrastructure planning and also may record potential fault activity in the region. Age constraints for these buried deposits are largely lacking and are needed for chronostratigraphic correlation, which in turn, supports hazard mitigation planning.

Tephra layers are preserved in deposits buried in the Sacramento–San Joaquin Delta (Maier et al., 2014). Abundant Quaternary volcanism in the western U.S. (Luedke and Smith, 1991) has led to sampling and analyses of numerous tephra layers from the region (Fig. 2), and results from thousands of samples are available in the U.S. Geological Survey (USGS) Tephrochronology Project database. The extent of primary tephra distribution, characteristics, geochemistry, and age constraints have been established for significant regional tephra (Fig. 2), including the Rockland ash bed (Sarna-Wojcicki et al., 1985; Lanphere et al., 2004) and the Loleta ash bed (Sarna-Wojcicki et al., 1987, 1989, 1991). Tephra are preserved and sampled in recent California Department of Water Resources geotechnical borehole cores in the Sacramento–San Joaquin Delta, potentially providing key chronostratigraphic markers.

In this study, we address these questions: 1) Which Quaternary tephra are preserved in buried deposits below the modern Sacramento–San Joaquin Delta?, 2) Do tephra record transport and deposition via fluvial processes?, and 3) Are individual tephra preserved or pervasively mixed with other tephra deposits? We hypothesize that individual tephra layers are preserved, and that a percentage of these tephra were primarily transported and widely deposited in fluvial systems, shortly following eruption, resulting in chronostratigraphic surfaces. Recognition of numerous new deposits of marker tephra buried below the modern Sacramento–San Joaquin Delta provides a temporal and spatial framework that supports interpretations of depositional environments and varying sediment accumulation rates. These new insights underpin subsurface correlations that will be an important part of future development, planning, and seismic hazard assessment in the Sacramento–San Joaquin Delta. Additionally, the identification, correlation, and depositional interpretation of tephra from geotechnical borehole samples here suggest that this integrated approach could also aid subsurface chronostratigraphic correlation in other fluvial-deltaic settings where geotechnical samples exist or where boreholes are being drilled.

Methods

Available existing data

From 2009 to 2012, the California Department of Water Resources (CDWR) drilled over 128 geotechnical boreholes across the Sacramento–San Joaquin Delta. The drilling was motivated by proposals to construct a subsurface water conveyance system along an approximate north–south-oriented alignment from south of Sacramento to Clifton Court Forebay (i.e., California Department of Water Resources et al., 2013). Geotechnical drilling and sampling procedure is described in Maier et al. (2014) and uses the Unified Soil Classification System (USCS) (American Society for Testing and Materials, 2007). During CDWR geotechnical drilling in the Sacramento–San Joaquin Delta, meters-thick units of white, angular, sand and silt-size grains, and rounded, pebble-size pumice grains were first recognized as potential tephra. Re-examination of geotechnical logs by CDWR following drilling led to additional recognition of potential tephra.

Geologic core descriptions and facies designations

In this study, CDWR cores were examined at centimeter scale to provide stratigraphic context for tephra samples and to document subtle differences in geologic parameters, such as grain size, sedimentary structures, Munsell color, etc. Geologic core descriptions followed methods detailed in Maier et al. (2014), wherein comprehensive logs of tephra-bearing cores and additional cores lacking tephra are also available. High-resolution logging was conducted for over 170 m of retained punch core samples from 27 boreholes in the northern and central regions of the delta in which tephra are identified. Detailed visual re-examination of punch core and SPT samples identified additional thinner, potential tephra-bearing units containing angular silt and sand-size grains, a characteristic texture, and generally, a lighter color than surrounding deposits.

Detailed observations in the form of geologic core logs, CDWR USCS logs, and CDWR photos are used to determine the thickness of tephra deposits, define tephra facies, and interpret processes of transport and deposition. Tephra deposits in the subsurface Sacramento–San Joaquin Delta are grouped into three facies based on grain size, thickness, and concentration of volcanic-derived grains. Variation within facies is described in terms of subfacies, which contain enough similar overall characteristics to be grouped as a single facies but display differing internal structures or subtle grain-size changes.

Tephra sampling and analyses

We use tephra nomenclature of Lowe (2008; 2011) wherein the term tephra encompasses volcanic ash (grains < 2 mm in diameter) and pumice lapilli (grains 2–64 mm in diameter). Both ash and pumice deposits contain volcanic glass shards < 2 mm in diameter. Potential tephra-bearing units were identified based primarily on a distinct texture, characteristic gray to white color, and presence of glass shards in the tephra units, in contrast to surrounding non-tephra-bearing deposits. Tephra units were also identified by the presence of large rounded pumice grains, distinct from sub-angular sand and gravelly sand deposits.

Ten tephra samples from eight of the 27 CDWR boreholes containing tephra were analyzed for glass shard chemistry (Fig. 1B, C; Table 1). Where possible, samples were obtained from punch cores in order to generate a high-resolution record of stratigraphic and depositional context. Six samples that each contained thick tephra deposits from depths ~40 m subsurface were analyzed from four boreholes near Hood, California. Three samples from three boreholes in the northern to central

https://doi.org/10.1016/j.yqres.2014.12.007 Published online by Cambridge University Press

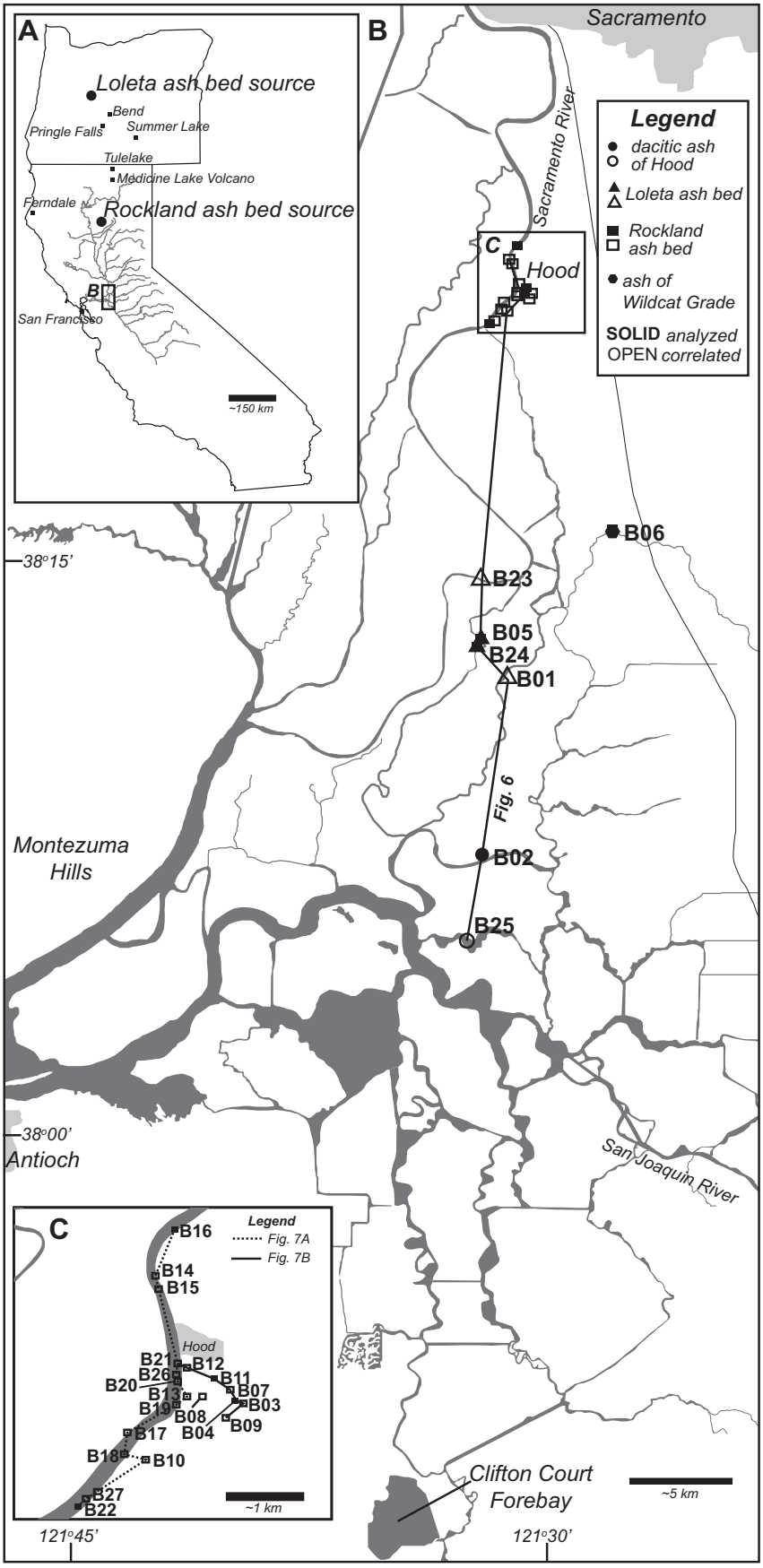

https://doi.org/10.1016/j.yqres.2014.12.007 Published online by Cambridge University Press

regions of the delta, south of Hood, were recovered from thinner tephra deposits at depths ranging from ~40 to ~53 m subsurface. One additional sample was recovered from an approximately 15-cm-thick tephra layer at ~60 m depth subsurface in the northeastern portion of the delta.

Tephra samples were processed, petrographically described, and analyzed with an electron microprobe in the USGS Tephrochronology Project and Microprobe laboratories in Menlo Park, California, generally following methods described in Sarna-Wojcicki et al. (1987) and McGann et al. (2013). Approximately 10 cm^3 was removed from the core or jar sample and washed with water through 100-, 200-, and 325-mesh (150 μ, 70 μ, and 38 μ, respectively) disposable nylon sieves to remove clay-size material. Next, the <150 μ to >70 μ fraction was treated with 10% dilute hydrochloric and 8% dilute hydrofluoric acids for 60 and 10 s, respectively, to remove any surface contamination and leached rims from volcanic glass shards. The volcanic glass shards were then separated from other tephra constituents using a Frantz magnetic separator (generally following Sarna-Wojcicki, 1976; Sarna-Wojcicki et al., 1979, 1984, 1987). Shards were embedded in an epoxy mount and polished to remove any altered exterior prior to electron microprobe analysis (EMPA).

Electron microprobe analysis (EMPA) utilized a JEOL8900 electron microprobe with a 10 micron beam diameter at 10 nA and the accelerating voltage set to 15.0 keV. For each sample, 20–30 grains were individually analyzed with EMPA to chemically fingerprint the tephra sample. Each shard was analyzed for nine major and minor element oxides (SiO_2 Al_2O_3, FeO (Fe_2O_3), MgO, MnO, CaO, TiO_2, Na_2O, K_2O). (See Supplementary Tables 1–10 for individual shard analytical results and descriptions.) Count time for sodium oxide is 10 s, and count times for other oxides are 20 s. We use ZAF matrix corrections to calculate oxide concentrations. The raw data were then recalculated to a 100% fluid-free basis. Relatively stable oxides of iron and calcium are plotted to show clustering of individual analyses in each analyzed sample (Fig. 3A), and analytical results are also illustrated in a total alkali ($Na_2O + K_2O$) silica (TAS) plot (after Le Bas et al., 1986) (Fig. 3B).

An average composition was calculated for each sample (with outliers removed) and quantitatively compared with a geochemical database of >6000 volcanic glass samples and a laboratory database of ~7500 processed samples, mainly from the western United States. For a complete tephrochronologic interpretation, geochemical data were considered in addition to independent age control, stratigraphic positions, field and petrographic characteristics, and mineralogy of the tephra sampled from Sacramento–San Joaquin Delta boreholes and reference tephra samples.

Results

General properties of tephra buried in the Sacramento–San Joaquin Delta

General types of tephra are identified as containing primarily volcanic ash, pumice, and volcanic-ash mixed with surrounding non-volcanic sediments. Tephra units are distinct in color and texture from non-volcanic deposits that dominate the core samples. Basal contacts of all tephra units identified in punch core samples are sharp, with the transition to tephra occurring over <1 cm. Upper contacts of tephra are generally a gradual transition into mixed layers of upward-decreasing tephra content.

Tephra were identified in 27 of the 128 recent CDWR boreholes (Table 1). These tephra layers ranged in thickness from ~0.1 m to ~7.5 m (average = 1.9 ± 1.7 m standard deviation) and were generally centered ~40 m, ~53 m, and ~60 m below the present ground surface in the northern, central, and eastern regions of the delta, respectively (Table 1). Tephra units occur at ~40 m depth in a number of closely spaced boreholes near the town of Hood, California (Fig. 1C), and at deeper depths in numerous boreholes drilled southward into the central region of the delta (Fig. 1B). Thick tephra deposits near Hood typically contain stacked layers that vary in volcanic ash content, grain size, and sedimentary structures. A single tephra unit occurs at ~60 m depth in the northeastern region of the delta, where few boreholes were drilled during 2009–2012.

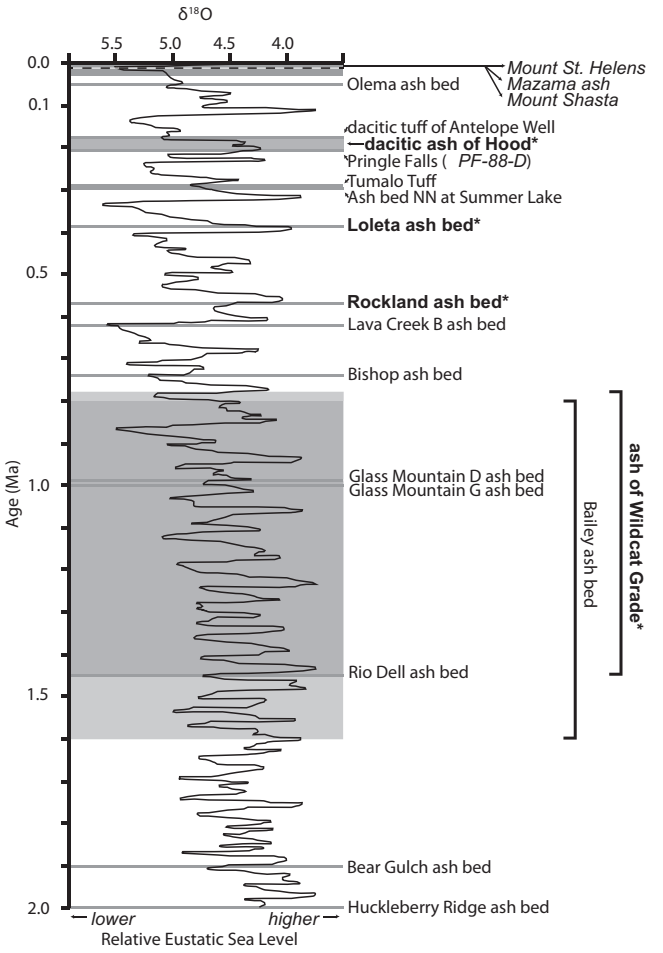

Figure 2. Stratigraphy of selected major regional tephra and tephra discussed in this study. Star and bold text indicate tephra identified in the subsurface Sacramento–San Joaquin Delta. Oxygen isotope and relative eustatic sea level curve from Murray-Wallace and Woodroffe (2014). Tephra ages from Taylor, 1981; Sarna-Wojcicki et al. (1985, 1987, 1989), Sarna-Wojcicki et al. (1991), Sarna-Wojcicki and Davis (1991) and references therein, and Lanphere et al. (2004). Rockland ash bed is represented with the tephrostratigraphic age (see text).

Tephra facies

We define three facies from tephra deposits in Sacramento–San Joaquin Delta boreholes based on grain size, thickness, concentration of volcanic-derived grains, and bedding structure. Tephra facies in the subsurface Sacramento–San Joaquin Delta include: 1) fluvial

Figure 1. Location of the Sacramento–San Joaquin Delta, California, study area and recent (2009–2012) California Department of Water Resources (CDWR) boreholes that intersect tephra deposits. A) Inset map showing the drainage area for water and sediment flowing into the modern Sacramento–San Joaquin Delta (box). The Rockland and Loleta ash beds, and the informally named dacitic ash of Hood (■,♦,●, respectively in Part B) identified in CDWR boreholes were erupted from volcanic sources to the north. The informally named ash of Wildcat Grade (■ in Part B) correlates to another Cascade sample from near Ferndale, coastal northern California. General locations of correlative samples from Pringle Falls, Bend, and Summer Lake, Oregon, and Tulelake and Medicine Lake Volcano, California, are indicated. B) Map of the modern Sacramento–San Joaquin Delta showing locations of tephra-bearing boreholes. Location of the correlation panel in Fig. 6 is indicated. C) Enlarged inset map of tephra-bearing boreholes near the town of Hood in the northern region of the delta. Locations of correlation panels in Fig. 7 are indicated.

https://doi.org/10.1016/j.yqres.2014.12.007 Published online by Cambridge University Press

Table 1
Tephra deposits in California Department of Water Resources (CDWR) Boreholes (2009–2012), Sacramento–San Joaquin Delta, California.

Borehole	CDWR ID	Data	Elevation (m)[1]	Top (m)[2]	Base (m)[2]	Thickness (m)	ID/*Stratigraphic Correlation*[2]	Facies	Underlying Deposit
B01	DCA-DH-003	Core, log	−1.3	−55.3	−56.1	0.8	*Loleta ash bed*	3b	Silt and clay
B02	DCA-DH-005	Core, log	−4.0	−38.8	−39.1	0.3	Dacitic ash of Hood (informal)	3a	Clayey silt and sand
B03	DCA-DH-014	Core, log	2.7	−39.6	−43.2	3.6	*Rockland ash bed*	2ab	Sand
B04	DCA-DH-024	Core, log	3.4	−40.1	−43.8	3.7	Rockland ash bed	1abcdefg	Sand
B05	DCA-DH-037	Log	0.8	−53.1	−53.3	0.2	Loleta ash bed	3	Silty sand
B06	DCE-DH-005	Log	1.2	−60.1	−60.3	0.2	Ash of Wildcat Grade (informal)	–	Clay
B07	DCIF-DH-013	Core, log	2.7	−41.0	−42.0	1.0	*Rockland ash bed*	1abcdfg	Sand
B08	DCIF-DH-014	Core, log	3.0	−40.1	−43.0	3.0	*Rockland ash bed*	2b	Silt, clay, and sand
B09	DCIF-DH-015	Core, log	2.6	−39.6	−42.2	2.6	*Rockland ash bed*	2bc	Silty sand
B10	DCN4-DH-009	Log	2.9	−40.7	−41.1	0.1	*Rockland ash bed*	–	Sand
B11	DCN4-DH-028	Core, log	2.9	−41.0	−43.1	2.1	Rockland ash bed	2a	Sand and gravel
B12	DCN4-DH-034	Core, log	3.6	−40.7	−43.1	2.4	*Rockland ash bed*	1acdfg	Sand
B13	DCN4-DH-036	Core, log	3.9	−40.8	−44.0	3.2	*Rockland ash bed*	1bcdeg	Sand
B14	DCR3-DH-003	Log	2.9	−42.7	−45.8	3.1	*Rockland ash bed*	2	Silty sand
B15	DCR3-DH-005	Log	3.0	−41.1	−41.9	0.8	*Rockland ash bed*	2	Silty sand
B16	DCR3-DH-013	Core, log	3.3	−39.9	−41.3	1.4	*Rockland ash bed*	1bcg	Clay
B17	DCR4-DH-004	Log	3.1	−41.9	−42.0	0.1	*Rockland ash bed*	3	Sand and silt
B18	DCR4-DH-006	Log	3.3	−41.3	−41.8	0.5	*Rockland ash bed*	3	Sand and silt
B19	DCR4-DH-013	Core, log	2.9	−41.2	−43.0	1.8	*Rockland ash bed*	1adcfebg	Sand
B20	DCR4-DH-014	Core, log	3.0	−40.5	−43.3	2.8	*Rockland ash bed*	1adec; 2a	Sand
B21	DCR4-DH-015	Core, log	3.0	−40.3	−42.5	2.2	*Rockland ash bed*	1cdg	Sand
B22	DCR5-DH-013	Core, log	2.8	−39.6	−47.1	7.5	Rockland ash bed	1b, 2acb	Sand and gravel
B23	DCRA-DH-002	Log	3.0	−51.8	−52.3	0.5	*Loleta ash bed*	3	Clay
B24	DCRA-DH-005	Core, log	1.7	−57.0	−57.2	0.2	Loleta ash bed	3c	Sandy clay
B25	DCRA-DH-009	Core, log	1.9	−52.2	−52.3	0.1	*Dacitic ash of Hood (informal)*	3a	Sandy clay
B26	DCR-DH-003	Log	1.6	−39.4	−42.0	2.6	*Rockland ash bed*	1	Silty sand
B27	DCR-DH-004	Log	1.5	−41.0	−44.7	3.7	*Rockland ash bed*	2	Silty sand

[1]of land surface or sediment–water interface; [2]drilled depth; [2]italicized indicates lithostratigraphic correlation; regular font indicates geochemically analyzed and correlated.
See Fig. 1 for borehole locations.

channel — concentrated volcanic ash, 2) fluvial channel — concentrated pumice, and 3) fluvial overbank — mixed volcanic ash and mud. All three facies contain volcanic glass shards, and Facies 2 also contains pumice.

Within each of the three facies, bed-scale variability is distinguished as subfacies. Facies 1 and 2 typically occur as two or more stacked tephra beds with varying sedimentary structures. Facies 3 occurs with varying thickness, typically with fewer stacked beds than Facies 1 or 2. Facies and subfacies are described here and interpreted in terms of depositional environments and transport processes.

Facies 1: fluvial channel — concentrated volcanic ash

Facies 1 has a characteristic white color (Munsell color 5Y 8/1) and is identified as volcanic ash, typically containing sand and silt (Table 2, Figs. 4A, 5A). Facies 1 deposits can be very thick (>3 m), and basal contacts generally occur above sand-rich non-volcanic deposits (Table 1). Many Facies 1 core samples display distinctive vertical stacking of basal, intermediate, and top units, each characterized by different sedimentary structures (Figs. 4A, 5A). Facies 1 subfacies are generally found in succession (i.e., Facies 1a, 1b, 1c, etc. from base to top), although all subfacies are not necessarily present in each borehole exposure (Table 1; Maier et al., 2014). Basal Facies 1 units are characterized by sand and silt-size volcanic ash and dark ferromagnesian minerals, such as hornblende, magnetite, and biotite (Facies 1a, Fig. 4A-F1a), and/or a very pure, concentrated deposit of silt-size volcanic ash (Facies 1b, Fig. 4A-F1b). Basal units of Facies 1 deposits may also contain internal deformation, such as water-escape structures or chaotic bedding (Facies 1c, Fig. 4A-F1c). Intermediate units in Facies 1 deposits often display structures such as parallel laminations and thin beds (Facies 1d, Fig. 4A-F1d) or ripple laminations and cross bedding (Facies 1e, Fig. 4A-F1e). Top units of Facies 1 deposits often display normal grading (Facies 1f, Fig. 4A-F1f) and reworking with non-volcanic siliciclastic detritus (Facies 1g, Fig. 4A-F1g).

Characteristics of Facies 1 deposits indicate rapid deposition from a flow containing concentrated tephra. Initial phases of Facies 1 deposition represented by massive Facies 1a and 1b indicate a flow with a high concentration of tephra material from which the grains were deposited too quickly to form sedimentary structures (e.g., Lowe, 1988). Continued rapid deposition of concentrated tephra material led to dewatering structures (e.g., Postma, 1983) and other internal deformation noted in Facies 1c. Variations in the order of appearance of Facies 1d and 1e may indicate fluctuations within the tephra-laden flow. Top units of Facies 1 deposits, displayed in Facies 1f and 1g, indicate a general decrease in flow energy (e.g., Miall, 1977b) and increasing mixing with non-tephra material. The final stage includes more non-volcanic material (i.e., reduced tephra concentration). Gradual transitions within tephra units, from pure or near-pure tephra to abundant (>~30%) volcanic ash mixed with non-volcanic sediments, are interpreted as a single tephra deposit and continuous depositional event containing a large and sudden influx of tephra material (e.g., Kataoka and Nakajo, 2002). Because this single depositional event is inferred to occur over a geologically short interval of time (e.g., Manville et al., 2005), Facies 1 deposits serve as chronostratigraphic markers in the subsurface Sacramento–San Joaquin Delta deposits.

Although the possibility of an air-fall volcanic ash component to some of the basal Facies 1 deposits cannot be completely eliminated due to the difficulty of distinguishing primary and reworked deposits (e.g., Leahy, 1997), structures and thickness of Facies 1 deposits suggest that fluvial transport brought tephra into the study area (e.g., Kataoka and Nakajo, 2002; Manville et al., 2005, 2009). Deposition in a confined setting, such as a fluvial channel, during flood events likely led to thick tephra deposits. Minimal subsequent scouring and erosion suggest that Facies 1 may not be deposited in the main fluvial channel thalweg, and may also involve oxbow lake environments. The occurrence of Facies 1 deposits at the same elevation within closely-spaced boreholes concentrated near Hood (Fig. 1C) and above sand-rich deposits (Table 1) supports the interpreted fluvial channel depositional environment.

Facies 2: fluvial channel — concentrated pumice

Facies 2 is defined as a mixture of medium-bedded (centimeter to decimeter bed thicknesses) pumice, volcanic ash, and non-volcanic siliciclastic sand often containing internal sedimentary structures (Table 2, Figs. 4B, 5B). Pumice grains are rounded and abraded. Facies 2 deposits are typically darker in color than Facies 1 deposits owing to

https://doi.org/10.1016/j.yqres.2014.12.007 Published online by Cambridge University Press

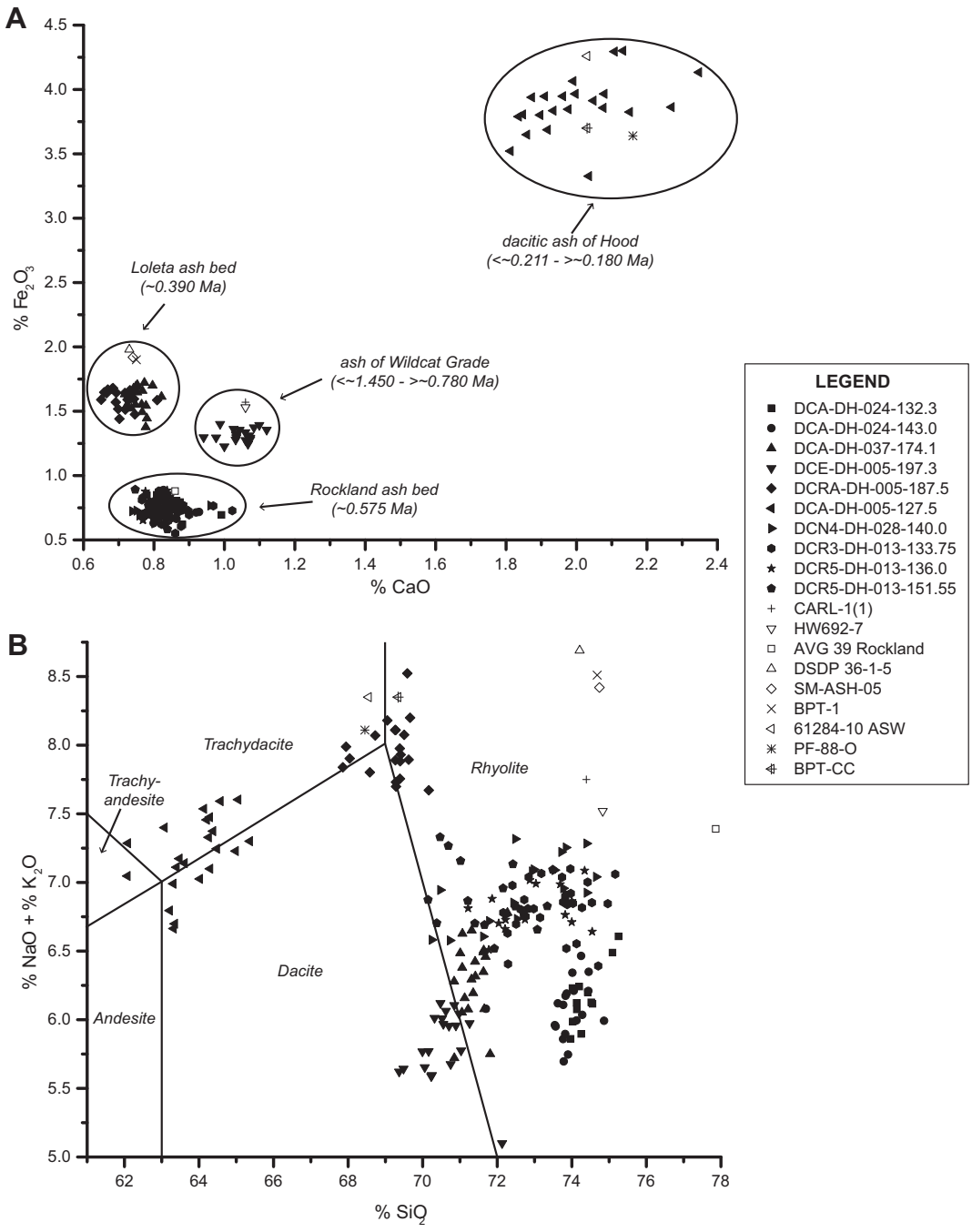

Figure 3. Plots of geochemical results from individual volcanic glass shard analyses of tephra samples from the Sacramento–San Joaquin Delta boreholes and database reference sample averages. See Table 3 and Supplementary Tables 1–10 for additional details. A) CaO vs. FeO plot. B) Total alkali silica (TAS) plot (after Le Bas et al., 1986).

greater abundance of pumice and non-volcanic sediments. Generally, Facies 2 deposits occur above finer-grained, less sand-rich deposits than Facies 1 (Table 1). Facies 2 deposits can also be very thick (>3 m) and occur as one or more subfacies.

Three subfacies of Facies 2 are differentiated based on grain size and sedimentary structures within pumice-rich deposits (Figs. 4B, 5B). Facies 2a consists of horizontal, medium-bedded, massive pumice-rich layers, generally without other internal structures (Fig. 4B-F2a). Facies 2b is comprised of abundant centimeter-thick cross-bedded, granule- to pebble-size pumice in medium-bedded, pumice-rich layers (Fig. 4B-F2b). Facies 2c is generally composed of finer-grained pumice, up to coarse sand size, and abundant silt-size tephra in medium-bedded units with centimeter-thick cross-bedding (Fig. 4B-F2c).

Deposition of Facies 2 occurred from a flow dominated by pumiceous sediment. Because individual pumice grains are rounded and abraded as is common from traction transport as bedload (e.g., Grabau, 1913; Miall, 1977a; Williams et al., 2013) and in fluvially transported tephra deposits (e.g., Manville et al., 2005), Facies 2 is interpreted to record a depositional event with enough energy to transport granule- to pebble-size pumice clasts as bedload. Thus, Facies 2 likely represents higher-energy conditions than those recorded by Facies 1 containing only silt and sand-size ash particles. Likewise, Facies 2c may represent slightly lower energy conditions than Facies 2a and 2b because Facies 2c includes coarse sand-size pumice grains and an overall finer average grain size.

https://doi.org/10.1016/j.yqres.2014.12.007 Published online by Cambridge University Press

Table 2
Tephra facies and sub-facies in the subsurface Sacramento–San Joaquin Delta, California.

Facies	Sub-facies	Description	Grain sizes	Sedimentary structures	Process implications	Depositional environment	Identified tephra
Concentrated volcanic ash							
1	1a	Massive sand-size ash with dark mineral grains	Sand and silt	None	Base of stratified flow Rapid deposition	Fluvial channel	Rockland ash bed
	1b	Massive silt-size ash	Silt	None	Rapid deposition		
	1c	Deformed silt-size ash	Silt	Chaotic bedding De-watering structures	Rapid deposition Soft sediment deformation		
	1d	Parallel laminated to thin-bedded ash	Silt	Low energy parallel laminations	Rapid deposition, slower than 1a, 1b, & 1c		
	1e	Cross-bedded to ripple laminated ash	Silt	Ripples Cross-bedding	Continued flow and decreased deposition rate from 1d		
	1f	Massive silt and clay-size ash	Silt and clay	None	Lower energy than 1e Continued rapid deposition		
	1g	Massive ash reworked with surrounding clay to sand	Clay and sand	Gradual upward decrease in tephra	Reworking		
Concentrated pumice							
2	2a	Flat-bedded pumice	Granule and pebble (*pumice*), Silt (*ash*), Sand	Medium-bedded massive pumice layers	High-energy Rapid deposition	Fluvial channel, thalweg	Rockland ash bed
	2b	Cross-bedded pumice	Granule and pebble (*pumice*), Silt (*ash*), Sand	Medium-bedded Cross-bedding	High-energy Rapid deposition Reworking		
	2c	Cross-bedded to ripple laminated pumice	Coarse sand (*pumice*) to silt (*ash*)	Medium-bedded Ripples Cross-bedding	Lower energy than 2b Deposition and reworking		
Mixed volcanic ash and mud							
3	3a	Thin (<0.5 ft), inclusion of non-volcanic grains, may display a pinkish color	Silt and clay	None	Rapid deposition Minor reworking	Fluvial overbank or flood plain; deposited by fluvial or air-fall mechanisms	Rockland ash bed; Loleta ash bed; dacitic ash of Hood
	3b	Reworked, silty	Silt and clay	Upward fining Upward decrease in ash content	Rapid deposition Reworking		
	3c	Massive, silty, white concentrated base, reworked top	Silt and clay	Upward fining Upward decrease in ash content	Stratified flow Rapid deposition Reworking		

Rapid deposition occurred in Facies 2, especially in Facies 2a massive beds (e.g., Lowe, 1988). All beds within Facies 2 are interpreted as a single tephra deposit and continuous depositional event owing to the concentration of pumice grains within these but not other deposits. Thus, Facies 2 deposits also serve as chronostratigraphic markers in the subsurface Sacramento–San Joaquin Delta deposits.

The abundant cross-bedding and thickness of Facies 2 suggest reworked tephra and fluvial transport into the Sacramento–San Joaquin Delta, similar to that interpreted for Facies 1. A confined setting, such as a fluvial channel, is interpreted for Facies 2 massive and cross-bedded pumice (e.g., Miall, 1977b; Kataoka and Nakajo, 2002; Manville et al., 2009). Facies 2 deposits likely are related to a primary flow path (i.e., fluvial channel thalweg) that received sediment-laden flows during a flood event (e.g., Manville et al., 2005). Like Facies 1, Facies 2 occurs exclusively in boreholes near Hood, and the silty underlying deposits (Table 1) may suggest that Facies 2 records a shift in a fluvial channel thalweg.

Facies 3: fluvial overbank — mixed volcanic ash and mud

Facies 3 is defined as volcanic ash mixed with non-volcanic siliciclastic sediments (Table 2, Fig. 4C). Facies 3 is generally lighter-colored than Facies 2 and slightly more gray or pink than Facies 1. Facies 3 deposits generally are thinner than Facies 1 or 2 deposits, and can be as thin as a few centimeters.

Figure 4. Photograph examples of tephra Facies 1, 2, and 3 from California Department of Water Resources geotechnical borehole core samples. A) Facies 1. Facies 1a (F1a): massive sand-size volcanic ash with dark mineral grains in core from borehole B12. Facies 1b (F1b): massive silt-size volcanic ash in core from borehole B04. Facies 1c (F1c): deformed silt-size volcanic ash in core from borehole B04. Facies 1d (F1d): parallel laminated to thin-bedded volcanic ash in core from borehole B20. Facies 1e (F1e): cross-bedded and ripple-laminated volcanic ash in core from borehole B20. Facies 1f (F1f): massive silt-to-clay size volcanic ash in core from borehole B07. Facies 1g (F1g): massive volcanic ash reworked with non-volcanic grains in core from borehole B21. B) Facies 2. Facies 2a (F2a): flat-bedded pumice in core from borehole B11. Facies 2b (F2b): cross-bedded pumice in core from borehole B09. Facies 2c (F2c): cross-bedded finer pumice in core from borehole B22. C) Facies 3 mixed volcanic ash and mud with sharp base contacts (arrows) to underlying sediments. Sub-facies are displayed from south to north, and photographs are shown at the same scale. Facies 3a (F3a): thin, partially reworked volcanic ash in core from borehole B02. Facies 3b (F3b): thicker volcanic ash deposit with reworked top in core from borehole B24. Facies 3c (F3c): thicker volcanic ash deposit with clean, white, concentrated base and reworked top in core from borehole B01.

https://doi.org/10.1016/j.yqres.2014.12.007 Published online by Cambridge University Press

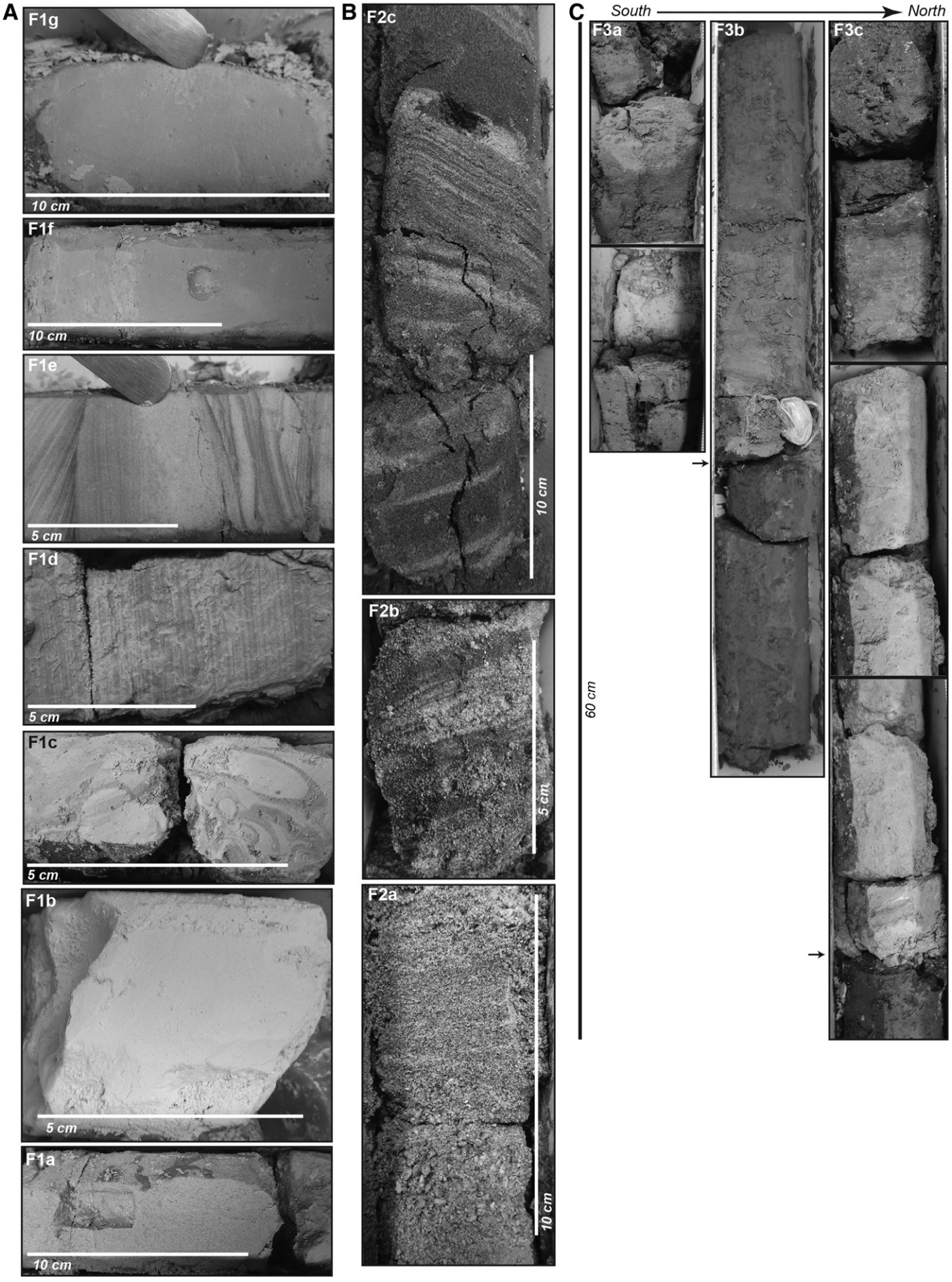

https://doi.org/10.1016/j.yqres.2014.12.007 Published online by Cambridge University Press

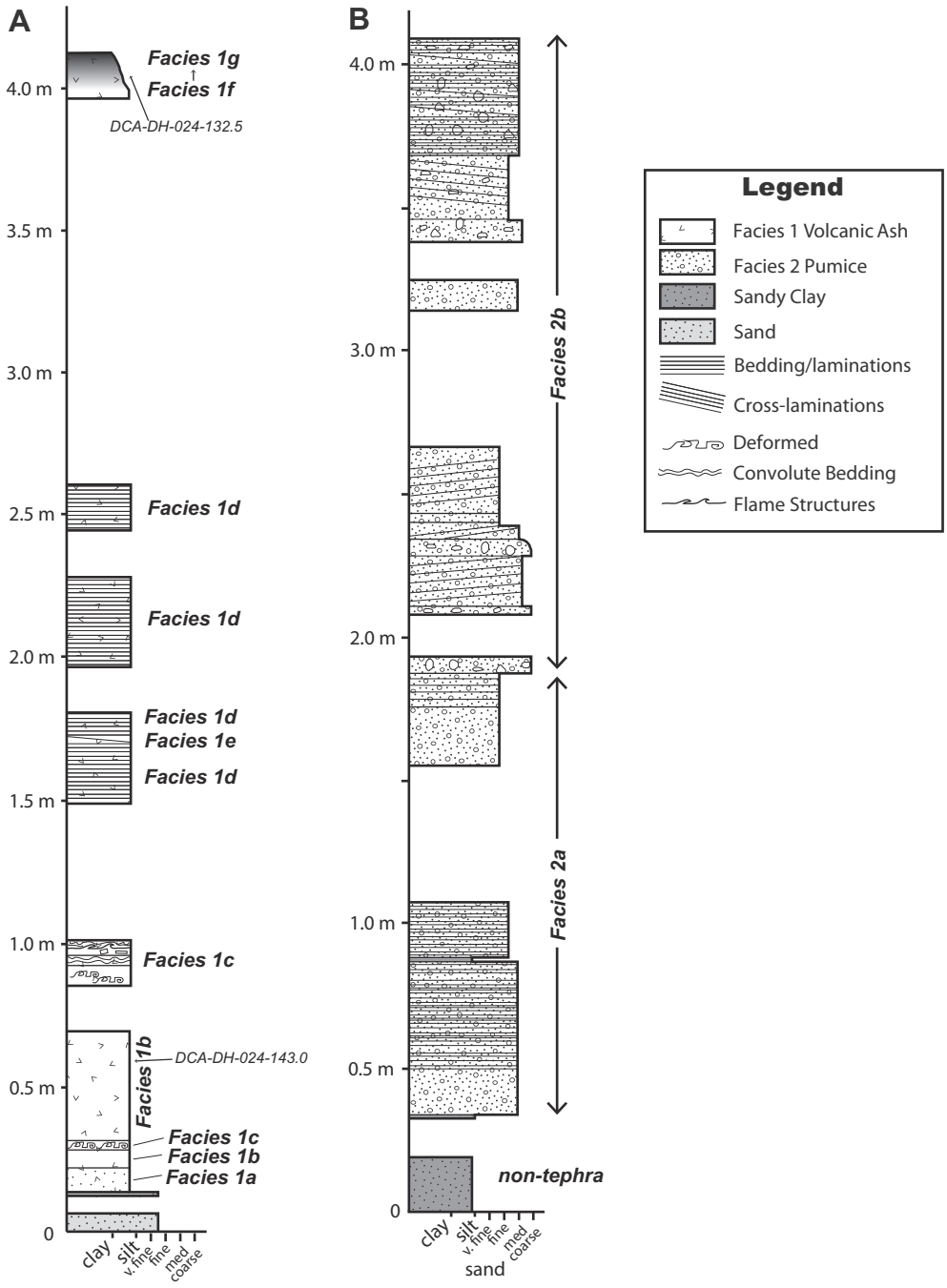

Figure 5. Graphic core log examples of Rockland ash bed facies and stacking of subfacies in California Department of Water Resources geotechnical borehole cores. A) Facies 1 in core samples from borehole B04. Stratigraphic locations of geochemically analyzed samples are indicated. B) Facies 2 in core samples from borehole B03.

Three subfacies are described from Facies 3 based on thickness and relative incorporation of non-volcanic grains. Facies 3a consists of a massive, thin (<30 cm total thickness) deposit of moderately concentrated silt-size volcanic ash with a characteristic pinkish appearance to pale olive-gray color (Munsell color 2.5Y 6/2) in core samples (Fig. 4C-F3a). This color may represent variation in tephra composition, surface contaminants or cements (such as clays, iron oxide, and carbonates) on grains, and sedimentary reworking as compared with other facies. Facies 3b lacks a concentrated tephra base and is a moderately thick (~1 m) zone of volcanic ash mixed with silt, sand, and clay (Fig. 4C-F3b). Facies 3c is a tephra deposit with a thin (<15 cm) massive white base of concentrated silt-size volcanic glass shards overlain by a thicker volcanic ash unit mixed with non-volcanic siliciclastic detritus (Fig. 4C-F3c). Both Facies 3b and 3c display an overall upward decrease in volcanic ash content.

The grain-size, structures, composition, and thickness of Facies 3 and deposits underlying Facies 3 suggest a lower energy, less confined depositional environment than Facies 1 and 2 (e.g., Miall, 1977b; Kataoka and Nakajo, 2002; Königer and Stollhofen, 2009; Manville et al., 2009). Facies 3a represents rapid deposition for a short time, potentially with less reworking than Facies 3b or 3c, owing to the lack of sedimentary structures other than grading. Like Facies 1a, the possibility of an air-fall component cannot be completely eliminated for concentrated volcanic ash in the base of Facies 3c (e.g., Leahy, 1997). Mixture with non-volcanic siliciclastic grains suggests that fluvial transport brought Facies 3 tephra into the study area. Unlike the thick tephra deposits of Facies 1

https://doi.org/10.1016/j.yqres.2014.12.007 Published online by Cambridge University Press

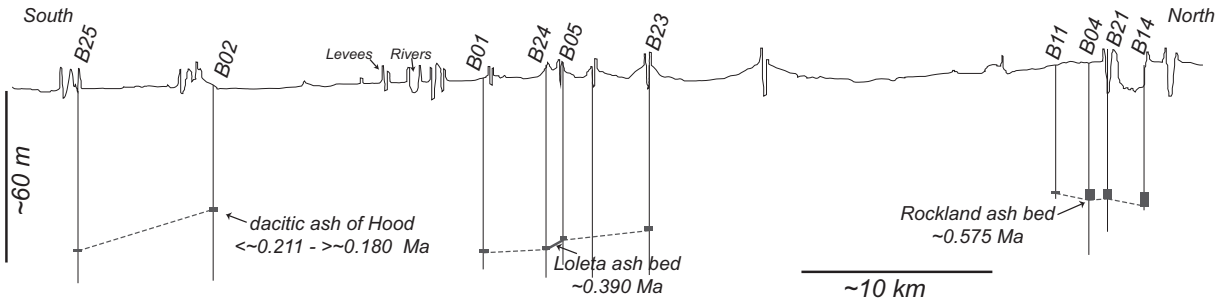

Figure 6. Correlation panel from the northern to central regions of the Sacramento–San Joaquin Delta showing the relative subsurface positions of tephra deposits in California Department of Water Resources (CDWR) boreholes. Quaternary deposits buried below the Sacramento–San Joaquin Delta appear to thicken to the south. See Fig. 1 for panel location. Boreholes are represented with vertical black lines, and tephra deposits are represented with gray boxes. Dashed lines indicate lithostratigraphic tephra correlations, and solid lines are geochemically correlated tephra. Topographic data generated by downsampling a LiDAR dataset provided by CDWR (2007–08 Sacramento–San Joaquin Delta LiDAR Acquisition).

and 2, Facies 3 does not require a confined depositional setting. Likely depositional environments for Facies 3 include fluvial overbank or floodplain settings that received periodic rapid deposition over large unconfined areas (e.g., Miall, 1977b; Kataoka and Nakajo, 2002; Königer and Stollhofen, 2009; Manville et al., 2009; Peterson et al., 2012). A floodplain to overbank setting is supported by the presence of fine-grained non-volcanic deposits consistently underlying Facies 3 (Table 1).

Facies associations

Boreholes in the Sacramento–San Joaquin Delta with tephra tend to contain a single Facies 1, 2, or 3 (Fig. 6). In the boreholes concentrated near Hood, lateral variations in facies occur over short distances (Fig. 7). Thin Facies 3 overbank deposits occur in two boreholes adjacent to channelized Facies 2 and 3 deposits, as would be expected for channel and overbank depositional environment facies associations. In the area of highest borehole density near Hood (Fig. 1C), Facies 2 generally occurs to the east of Facies 1 (Fig. 7), likely related to the interpreted channel and avulsed channel deposits.

Facies 1 and 2 are documented in vertical succession in only two boreholes, B20 and B22, where inconsistent superposition of Facies 1 and 2 suggests that a single event transported pumice and other finer-grained tephra together. In B20, basal massive volcanic ash is overlain by at least two units of tephra with basal pumice beds. These may represent fining upward packages, common in fluvial deposits, and alternating pumice and finer-grained deposition. Fluvial drainages likely provided a mixture of volcanic glass shards and pumice that was stratified and/or experienced staggered arrival in the Hood area. Borehole B22 contains an upward increase in grain size and cross-bedding where pumice followed volcanic ash deposition (Fig. 7), indicating an increase in flow energy through time or a later arrival of pumice laden tephra derived from drainages located closer to the eruptive center.

Tephra analytical results

The chemistry of samples from each of the three tephra facies in this study was analyzed and compared to reference tephra samples in the western U.S. (Table 3, Fig. 3, Supplementary Tables). Four separate tephra are recognized in the CDWR boreholes and associated with age constraints based on prior studies. Here, the four tephra are presented in stratigraphic order from oldest to youngest.

Informally named ash of Wildcat Grade (<~1.450 to >~0.780 Ma)

The normalized compositions of volcanic glass shards from sample DCE-DH-005-197.3 in CDWR borehole B06 show this to be a homogeneous volcanic ash (Supplementary Table 4). The bulk sample had a dry Munsell color of light olive gray (5Y 6/1). Glass shard morphology indicates the presence of ~90% well-hydrated, platy, finely to coarsely ribbed, or bubble wall/bubble wall junction shards that are solid to well-vesiculated with elongate cylindrical or equant to irregular bubble-type vesicles. Approximately 4% of constituents are highly devitrified grains.

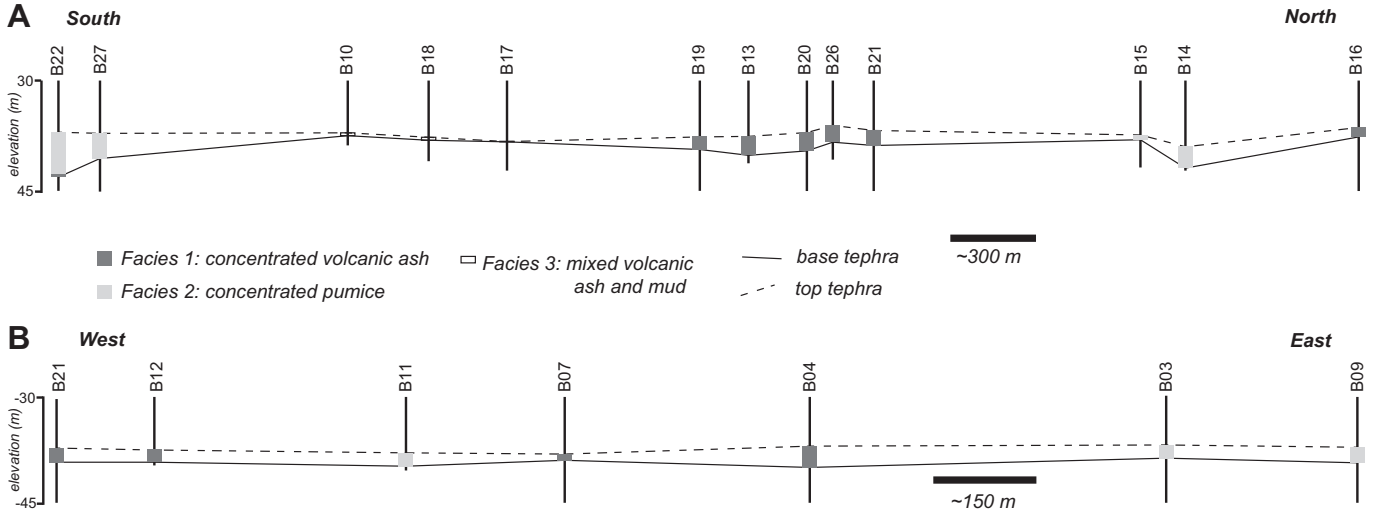

Figure 7. Correlation panels of Rockland ash bed deposits in boreholes near Hood. Facies 1 and 2 record channelized deposits, and thin Facies 3 deposits represent overbank depositional environments. See Fig. 1 for panel locations. A) North–south oriented cross-section approximately paralleling the modern Sacramento River. B) East–west oriented cross-section.

https://doi.org/10.1016/j.yqres.2014.12.007 Published online by Cambridge University Press

The remainder of the sample is composed of minor percentages of feldspars, quartz, orthopyroxenes, amphiboles, and biotite.

Based on geochemical data, in addition to independent age control for previously analyzed reference samples, stratigraphic context, field and petrographic characteristics, and mineralogy, this tephra in borehole B06 is most closely associated with samples CARL-1(1) and HW692-7 in the USGS Tephrochronology Project database (Table 3; Fig. 3A). HW692-7 is a tuff from the Montezuma Formation (Graymer et al., 2002) exposed in the Montezuma Hills, California, located ~30 km west of borehole B06. CARL-1(1) is an un-named, Cascade-type Pleistocene tephra from near the base of the Carlotta Formation on Wildcat Ridge along Mattole Road, about a mile south of Ferndale, coastal northern California (Fig. 1A). Ogle (1953) referred to this tephra as the Carlotta ash. The Wildcat Grade ash is another informal name given to this tephra by S. Morrison of the Bureau of Land Management (personal communication). In this study, DCE-DH-005-197.3 will hereafter be referred to as the informally named ash of Wildcat Grade.

Sarna-Wojcicki et al. (1987) demonstrated that CARL-1(1) overlies the Rio Dell ash bed (~1.450 Ma) contained in the underlying Rio Dell Formation. CARL-1(1) also underlies the Rockland ash bed (~0.575 Ma), which is present and exposed in the overlying Hookton Formation (Sarna-Wojcicki et al., 1991). The ~0.780 Ma Brunhes Normal-Polarity Chron–Matuyama Reversed-Polarity Chron boundary occurs near the base of the Hookton Formation (Woodward-Clyde Consultants, 1980), further constraining the minimum age range of CARL-1(1) as older than ~0.780 Ma. Previous studies also have found the Brunhes–Matuyama boundary preserved in time-transgressive strata disconformably overlying the Rio Dell Formation (Clifton and Leithold, 1991). Based on the above geochemical correlations and stratigraphic interpretations, CARL-1(1), and thus DCE-DH-005-197.3 and the ash of Wildcat Grade, have an age of between ~1.450 Ma and ~0.780 Ma.

Rockland ash bed (~0.575 Ma)

Six tephra samples (DCA-DH-024-132.3, DCA-DH-024-143.0, DCN4-DH-028-140.0, DCR3-DH-013-133.75, DCR5-DH-013-136.0, and DCR5-DH-013-151.55 in boreholes B04, B11, B16, and B22, respectively) from near Hood in the northern region of the delta display overall similarities in geochemistry, subsurface depth, petrography, and mineralogy. Samples from near the bases of the associated tephra units are fairly homogeneous with a relatively high percentage of glass versus mineral and altered grains, and lithic fragments. For example, sample DCA-DH-024-143.0 (bulk sample Munsell color: yellowish gray (5Y 8/1)) contains ~82% moderately coated (clay and iron oxide), predominantly colorless (rarely light brown), platy or blocky glass shards occasionally with bubble wall/bubble wall junctions or fine, straight ribs, and equant to irregular bubble-type or elongate tubular vesicles. Some microlitic shards were also observed along with a small subpopulation of highly frothy pumiceous shards. Remaining sample constituents include comagmatic plagioclase feldspar, quartz, devitrified grains, hypersthene, hornblende, magnetite, biotite, and microphenocrysts of apatite.

Samples from the tops of tephra units are more heterogeneous, polymodal, and hydrated. For example, sample DCA-DH-024-132.3 (bulk sample Munsell colors: yellowish gray (5Y 7/2) to light olive gray (5Y 5/2)) contains two geochemical populations of glass shards (see Supplementary Table 1). Compared to near basal sample DCA-DH-024-143.0, the residue from the DCA-DH-024-132.3 contains a lower percentage (~56%) of colorless to light brown shards.

Table 3
California Department of Water Resources (CDWR) Sacramento–San Joaquin Delta (California) borehole tephra volcanic glass shard compositions determined by electron microprobe, chemical correlatives, and approximate age determinations.
Identified tephra are listed in stratigraphic order, from oldest to youngest, along with eruptive source areas and close chemical correlatives. Values are weight-percent oxide, recalculated to 100% fluid free basis. Twenty to thirty grains were analyzed per sample.

SAMPLE ID	SiO_2	Al_2O_3	Fe_2O_3	MgO	MnO	CaO	TiO_2	Na_2O	K_2O	LOCATION
Ash of Wildcat Grade, informal name, this study (<~1.450 to >~0.780 Ma); volcanic source area: Cascade Range, Oregon										
DCE-DH-005-197.3 (B06)	75.45	15.08	1.57	0.27	0.08	1.12	0.21	3.52	2.71	Eastern Sacramento–San Joaquin Delta, Sacramento County, California
CARL-1(1)	74.39	14.72	1.57	0.26	0.05	1.06	0.20	4.83	2.92	Carlotta Fm., Wildcat Ridge, Humboldt County, California
HW692-7	74.83	14.53	1.53	0.26	0.08	1.06	0.19	4.62	2.90	Montezuma Hills, Solano County, California
Rockland ash bed (~0.575 Ma), average of 39 samples; volcanic source area: Lassen Peak area, California										
AVG 39 ROCKLAND TEPHRA	77.86	12.65	0.88	0.17	0.03	0.86	0.16	3.79	3.60	Volcanic source area: southern Cascade Range in vicinity of Lassen Peak, Shasta County, California (Sarna-Wojcicki and Davis, 1991)
DCA-DH-024-132.3 (B04)	78.37	12.96	0.90	0.17	0.05	0.89	0.17	2.98	3.51	Near town of Hood, Sacramento County, California
DCA-DH-024-143.0 (B04)	78.42	12.98	0.88	0.19	0.03	0.89	0.16	2.96	3.49	Near town of Hood, Sacramento County, California
DCR3-013-133.75 (B11)	77.90	12.79	0.86	0.16	0.03	0.89	0.16	3.60	3.62	Near town of Hood, Sacramento County, California
DCR5-013-136.0 (B16)	77.91	12.72	0.89	0.15	0.03	0.88	0.16	3.66	3.60	Near town of Hood, Sacramento County, California
DCR5-013-151.55 (B22)	77.76	12.64	0.91	0.15	0.04	0.88	0.15	3.78	3.70	Near town of Hood, Sacramento County, California
DCN4-028-140.0 (B22)	77.78	12.73	0.84	0.16	0.03	0.88	0.15	3.75	3.67	Near town of Hood, Sacramento County, California
Loleta ash bed (~0.390 Ma, distal equivalent of Bend Pumice), volcanic source area; Three Sisters (?), central Cascade Range, Oregon										
DCRA-DH-005-187.5	74.34	14.12	1.91	0.10	0.06	0.76	0.15	5.32	3.24	Northern Sacramento–San Joaquin Delta, Sacramento County, California, Moderately to well hydrated sample.
DCA-DH-037-174.1	75.88	14.37	1.89	0.13	0.07	0.81	0.15	3.66	3.05	Northern Sacramento–San Joaquin Delta, Sacramento County, California, Moderately to well hydrated sample.
DSDP 36-1-5 (57 cm)	74.21	14.07	1.98	0.12	0.06	0.73	0.14	5.42	3.27	Deep Sea Drilling Site 36, northeast Pacific Ocean, offshore California
SM-ASH-05	74.74	13.86	1.92	0.10	0.06	0.74	0.17	5.28	3.14	East of town of Loleta, Humboldt County, California
BPT-1	74.68	13.81	1.90	0.12	0.07	0.75	0.16	5.22	3.29	Bend Pumice = near source equivalent; volcanic source area: Three Sisters(?), central Cascade Range, Oregon
Dacitic ash of Hood, informal name, this study (<~0.211 to >~0.180 Ma, $^{40}Ar/^{39}Ar$ isochron age, Singer et al., 2008); volcanic source area: southern Cascade Range, Oregon										
DCA-DH-005-127.5	68.14	15.98	4.60	0.67	0.13	2.14	0.65	5.37	2.32	Central Sacramento–San Joaquin Delta, Sacramento County, California, Moderately to well hydrated sample.
61284-10	68.55	15.37	4.26	0.66	0.14	2.03	0.65	5.85	2.50	Tulelake basin, near Deadhorse Gulch, Modoc County, California. Underlies 61284-14 (Sarna-Wojcicki, unpublished data), the ~0.180 Ma tuff of Antelope Well (Donnelly-Nolan, 2010)
BPT-CC	69.34	15.31	3.70	0.72	0.12	2.03	0.65	5.85	2.50	Columbia Canal site, Deschutes County, Oregon. airfall pumice lapilli overlying ~0.290 Ma Tumalo Tuff (Sarna-Wojcicki et al., 1989).
PF-88-O (SILICIC)(2)	68.45	16.19	3.64	0.67	0.11	2.16	0.67	5.81	2.30	Pringle Falls, Deschutes County, Oregon. PF-88-O stratigraphically overlies PF-88-D (~0.211 Ma, Ar/Ar isochron age, Singer et al., 2008)

https://doi.org/10.1016/j.yqres.2014.12.007 Published online by Cambridge University Press

Furthermore, the glass separate in this sample is composed of lower density, lightly to heavily coated (iron oxide, carbonate, and clay), finely ribbed and webby/frothy pumiceous shards containing equant to irregular bubble-type vesicles. Bubble-wall/bubble wall junction shards, platy, and coarsely ribbed shards are less common. The remainder of the processed residue consists of ~34% devitrified grains, and ~10% euhedral to subhedral, occasionally glass-coated minerals, including hypersthene, biotite, plagioclase, quartz, hornblende, magnetite, and microphenocrystic apatite.

The six tephra samples near Hood are interpreted to correlate with the Rockland ash bed based on the geochemical similarity of these samples with average Rockland ash bed chemistries (Table 3; Fig. 3A), independent age control, stratigraphic positions, field and petrographic characteristics, and mineralogy. The Rockland ash bed erupted in the southern Cascades, southeast of Mount Lassen in northern California and has been extensively studied in the Pacific northwest region (Fig. 1A; Sarna-Wojcicki et al., 1985; Lanphere et al., 2004). Argon ($^{40}Ar/^{39}Ar$) and U/Pb ages range from 0.609 ± 0.007 Ma to 0.565 ± 0.012 Ma (Lanphere et al., 2004), and ~0.575 Ma is used here as the tephrostratigraphic age. The Rockland ash bed is a thick lithologic unit in both boreholes B04 and B22, and samples spaced meters-apart in each of these boreholes are interpreted as representing the bases (DCA-DH-024-143.0 and DCR5-DH-013-151.55) and reworked tops (DCA-DH-024-132.3 and DCR5-DH-013-136.0) of Rockland ash bed deposits.

Loleta ash bed (~0.390 Ma)

Tephra samples DCA-DH-037-174.1 and DCRA-DH-005-187.5 in boreholes B05 and B24, respectively, display fairly homogeneous geochemistry, with the exception of NaO (Table 3; Fig. 3). DCA-DH-037-174.1 (bulk sample Munsell color: olive gray (5Y 3/2)) contains ~72% platy or finely ribbed glass shards. Some of the shards display moderately to well-hydrated, tubular, and (or) equant to irregular bubble-type vesicles, and some also have randomly oriented microlites. The sample additionally contains ~21% highly altered and devitrified grains, ~5% feldspars and quartz, ~1% hypersthene, hornblende, and biotite.

Sample DCRA-005-187.5 (bulk sample Munsell color: light olive gray (5Y 6/1)) is predominantly comprised of ~79% angular, colorless, platy, tightly ribbed, or bubble wall/bubble-wall junction, and sparsely vesiculated shards. Microlites are noted in some of the shards. Webby shards, and unhydrated to poorly hydrated, nearly to perfectly spherical single bubble shards are much less common. Observed mineral assemblage includes feldspars, quartz, hornblende, biotite, and possibly chlorite. This is consistent with the percent abundance and shard morphology observed in sample DCA-DH-037-174.1.

Geochemical data from tephra deposits in boreholes B05 and B24 compared with the USGS Tephrochronology Project database, in addition to independent age control for database samples, stratigraphic positions, field and petrographic characteristics, and mineralogy, suggest geochemical correlation with multiple previously analyzed samples of the Loleta ash bed (~0.390 Ma). These previously analyzed samples include offshore samples from the Pacific margin and northeast Pacific Ocean, including tephra intervals in Deep Sea Drilling Project (DSDP) Site 36 in the northeastern Pacific Ocean (Sarna-Wojcicki et al., 1987; Wan, 1988). The database also includes analyzed samples of Bend Pumice (Sarna-Wojcicki et al., 1987) from Bend and Pringle Falls, Oregon (Sarna-Wojcicki et al., 1987, 1989, 1991), and samples from Humboldt Basin, California, among other distal localities (Table 3; Fig. 3A). The Loleta ash bed is thought to have erupted from the central Cascades of Oregon, possibly from the Three Sisters volcanoes, and is the distal equivalent of the Bend Pumice, near Bend, Oregon (Sarna-Wojcicki et al., 1987, 1989, 1991) (Fig. 1A).

Informally named dacitic ash of Hood (<0.211 to >0.180 Ma)

Tephra sample DCA-DH-005-127.5 in borehole B02 is from a thin (<0.1 m-thick) layer of well-sorted, very fine-grained, pinkish to pale olive-gray silt. The sample (bulk sample Munsell color: yellowish gray (5Y 7/2)) contains ~75% colorless to medium brown colored, microlitic or microphenocrystic glass shards that are commonly platy, or exhibit bubble wall/bubble-wall junctions, ribs, and vesicles. The microlites and microphenocrysts are oriented randomly, parallel following ribbing, or rarely in a radiating pattern.

Glass shards in sample DCA-DH-005-127.5 are similar to dacitic–andesitic volcanic glass samples from Cascade-type tephra found at Tulelake, California, and Pringle Falls, Bend, and Summer Lake, Oregon. Sample DCA-DH-005-127.5 mostly closely correlates with sample 61284–10 ASW (Table 3; Fig. 3A) from Tulelake basin, near Deadhorse Gulch, Modoc County, California. Sample 61284–10 ASW underlies sample 61284–14 ASW, which in turn, correlates to the dacite tuff of Antelope Well (A. Sarna-Wojcicki, unpublished data) and previously named "andesite tuff" by C.A. Anderson (Donnelly-Nolan, 2010). The dacite tuff of Antelope Well has a reported age of ~0.180 Ma and originated from Medicine Lake Volcano in northern California (Herrero-Bervera et al., 1994; Donnelly-Nolan, 2010) (Fig. 1A). Sample DCA-DH-005-127.5 is also closely associated with PF-88-O (Table 3; Fig. 3A), a tephra from a stratigraphic section in Pringle Falls, Oregon, that overlies PF-88-D, which has an $^{40}Ar/^{39}Ar$ isochron constrained age of 0.211 ± 0.0064 Ma (Singer et al., 2008). These correlations thus bracket the age range of sample DCA-DH-005-127.5 as between <~0.211 to >~0.180 Ma. Further support that sample DCA-DH-005-127.5 is a middle Pleistocene tephra is provided by its similarity to BPT-CC, a tephra from Columbia Canyon, Oregon that overlies the ~0.290 Ma Tumalo Tuff (Sarna-Wojcicki et al., 1989) (Table 3). BPT-CC in turn is chemically similar to ash bed NN at Summer Lake, Oregon (Sarna-Wojcicki et al., 1989) which also has an $^{40}Ar/^{39}Ar$ age of ~0.300 Ma (Donnelly-Nolan et al., 2004).

Discussion

Tephra correlations

Tephra deposits in the subsurface of the Sacramento–San Joaquin Delta provide the most reliable chronostratigraphic markers owing to their rapid deposition in concentrated discrete layers with distinguishable facies. Comparison of analyzed samples with an extensive database including samples that have been studied from better-preserved and exposed deposits throughout the region provides reasonable and reliable age constraints for each of the four tephra identified in this study that could not be derived from CDWR borehole samples alone. Using facies analyses, tephra correlations are broadly interpreted in unanalyzed samples and used to delineate chronostratigraphic surfaces below the modern Sacramento–San Joaquin Delta.

Identification of the Rockland ash bed, the Loleta ash bed, and the dacitic ash of Hood can be tentatively extended based on facies characteristics and stratigraphic position, thus extending age constraints and chronostratigraphic markers. In this study, Facies 1 and 2 occur exclusively in Rockland ash bed deposits near Hood at similar depths, allowing inferred lithostratigraphic recognition of the Rockland ash bed in 19 additional boreholes with unanalyzed tephra deposits (Table 1; Figs. 1, 6, 7). Facies 3 has been identified intermittently in the northern to central regions of the study area and individual Facies 3 deposits are associated with the Rockland ash bed, the Loleta ash bed, and the dacitic ash of Hood. The Loleta ash bed only occurs as Facies 3b and 3c, and the Loleta ash bed correlations are tentatively extended to three additional boreholes with unanalyzed Facies 3 tephra deposits at similar depths (Figs. 1, 6). Thin tephra beds of Facies 3a occur farthest to the south, in the central region of the delta where the dacitic ash of Hood is encountered. Deposits of the dacitic ash of Hood that occur in borehole B02 as Facies 3a are very similar to a tephra deposit in borehole B25 to the south. Although the tephra layer occurs at a much lower depth in B25 than in B02, they are both reasonably inferred to be the same tephra based on strikingly similar and distinct appearance.

https://doi.org/10.1016/j.yqres.2014.12.007 Published online by Cambridge University Press

Correlation of individual named tephra in adjacent boreholes records subtle variations in paleotopography, faulting, or differential subsidence (Fig. 6). Loleta ash bed samples have ~3 m of topographic variation on the chronostratigraphic surface marked by the base of the tephra over ~8 km. The Rockland ash bed, identified across ~>15 km^2 (Fig. 1C) has a relatively planar basal contact with ~3 m variation, possibly connected to local channel-related erosion. Differential depths of the dacitic ash of Hood are interpreted to be related to differential subsidence between the northern and central portions of the delta.

Identification of tephra chronostratigraphic markers in the subsurface allows stratigraphic correlation in the study area with other deposits in the region and along the Pacific margin. Identification and correlation of tephra are particularly important in complicated tectonic settings like California, where time-correlative deposits may occur at different elevations over short distances. For example, the Montezuma Hills, a fault-bounded horst located at the western edge of the Sacramento–San Joaquin Delta (Krug et al., 1992), contain a tuff that correlates with the ash of Wildcat Grade sampled at ~60 m subsurface depth in the eastern region of the delta (Table 3), which provides evidence that the hills contain sediment equivalent in age to sediment buried below the eastern region of the delta. Thus, a portion of the section encountered near the base of borehole B06 may be correlative with the Montezuma Formation (Graymer et al., 2002). Additionally, identification of widespread tephra, like the Rockland and Loleta ash beds, relates deposits in the Sacramento–San Joaquin Delta to other basins and outcrops across the Pacific northwest region and to more complete stratigraphic sections in DSDP Site 36 (e.g., Sarna-Wojcicki et al., 1987, Wan, 1988, Sarna-Wojcicki et al., 1989, 1991; Lanphere et al., 2004).

Tephra depositional environments and preservation

Based on inferred types of depositional environments in the region during the Quaternary, borehole locations in the modern Sacramento–San Joaquin Delta, first-order depositional interpretations of tephra facies in this study, and relative eustatic sea level for approximate ages of identified tephra in this study (Fig. 2), fluvial depositional environments are interpreted for tephra buried below the modern Sacramento–San Joaquin Delta. During sea-level lowstands, the study area was likely dominated by braided or meandering fluvial channels (e.g., Barnard et al., 2013 and references therein). At sea-level highstands, the region may have contained fluvial, lacustrine, estuarine, and tidal marsh environments (e.g., Malamud-Roam et al., 2006; Dettinger and Ingram, 2013; Drexler et al., 2014). Combined analysis of tephra facies and geochemistry helps to refine interpretation of deposits relative to fluctuations in Quaternary eustatic sea level (e.g., Murray-Wallace and Woodroffe, 2014; Fig. 2).

Tephra Facies 1 and 2 interpretations in combination with eustatic sea-level lowstand conditions during eruption (i.e., Bassinot et al., 1994; Fig. 2) lead to an interpretation of Rockland ash bed deposits being brought into the study area via fluvial transport from drainages closer to the volcanic source area (Fig. 1A). Although fluvial transport of the Rockland ash bed has not received as much attention as the age and geochemistry of this tephra (e.g., Sarna-Wojcicki et al., 1985; Lanphere et al., 2004; Pouget et al., 2014), fluvial transport and sedimentation of fine-grained and pumice-rich tephra are common in other settings (e.g., Shane, 1991; Mack et al., 1996; Kataoka and Nakajo, 2002). Fluvial transport mechanisms may warrant consideration throughout the region of Rockland ash bed occurrence, especially when interpreting isopach maps (e.g., Pouget et al., 2014). Proximal and distal Rockland ash bed deposits are known to contain both pumice tuff breccia and finer-grained flow components with some reworking (Sarna-Wojcicki et al., 1985; Lanphere et al., 2004). Both appear to be present in the study area. We interpret the Rockland ash bed transport and deposition in the Sacramento–San Joaquin Delta as the result of a large flood event in the paleo-Sacramento River, perhaps similar to Holocene and historic flood events in the Sacramento–San Joaquin Delta and its drainages (e.g., Malamud-Roam et al., 2006; Dettinger and Ingram, 2013; Drexler et al., 2014). Such flood events would have widespread impact and may be relevant to other Rockland ash bed deposits in the region.

Limited borehole sampling beyond Hood restricts depositional environment interpretations for the Loleta ash bed, the dacitic ash of Hood, and the ash of Wildcat Grade in the Sacramento–San Joaquin Delta. In general, thin, fine-grained Facies 3 deposits likely represent deposition in overbank environments from fluvial transport (e.g., Kataoka and Nakajo, 2002; Königer and Stollhofen, 2009; Manville et al., 2009; Peterson et al., 2012). Where Facies 3 deposits occur adjacent to thicker fluvial channel deposits of the Rockland ash bed, they are interpreted as fluvially transported overbank deposits of the Rockland ash bed. The Loleta ash bed and the dacitic ash of Hood may have been deposited during higher eustatic sea level conditions than the Rockland ash (Fig. 2) but may still represent fluvial depositional environments. Broad age constraints for the informally named ash of Wildcat Grade span numerous sea level fluctuations (Fig. 2), and lack of retained cores prohibits further depositional environment interpretations.

The spatial distribution and preservation of all four tephra deposits identified in this study are functions of the location of existing subsurface data, variations in sediment thickness within the subsurface chronostratigraphic packages relative to borehole penetration depths, varying environments of tephra deposition, and preservation potential. The older ash of Wildcat Grade is present only in a deep borehole in the eastern region of the delta, where the overall Quaternary sediment package is thinner. Likewise, the Rockland ash bed is present in deep (>40 m) boreholes in the Hood area but not farther south, where boreholes are not drilled deep enough to intersect time-correlative sediment packages that might contain Rockland ash bed deposits (Fig. 6). A dynamic depositional environment with frequent fluvial erosion, especially during low stands of sea level, leads to an overall low preservation potential for tephra in the study area, yet prevalent tephra deposits are identified in borehole data presented here and may be related to large influx of tephra during flood events. Channel avulsion related to rapid deposition during tephra-laden flood events may have contributed to preservation of Rockland ash bed deposits. The Loleta ash bed and younger dacitic ash of Hood occur as thin layers, and they are missing from many adjacent boreholes with time correlative packages, likely due to the overbank depositional environment that may have experienced erosion or limited tephra deposition (e.g., Königer and Stollhofen, 2009; Peterson et al., 2012). Tephra that occur as thin Facies 3 deposits may be present but unrecognized in additional boreholes where core samples were not taken or were not retained. Continued drilling coupled with targeted core sampling could potentially identify more tephra (e.g., Fig. 2) and extend tephra chronostratigraphy in the region. Additionally, the utility of tephra in this study suggests that geotechnical borehole data from other locations could be useful in identifying tephra and correlating chronostratigraphic surfaces, even when tephra deposits are reworked. In particular, other mid-latitude regions with documented Quaternary volcanism and potential for flood events may preserve tephra deposits in channel, overbank, and lacustrine environments.

Quaternary sediment accumulation rates

Lack of a simple linear relationship between age and depth of tephra deposits indicates variation of Quaternary sediment thickness within the Sacramento–San Joaquin Delta. In particular, the younger ~0.390 Ma Loleta ash bed is identified at deeper depths than the ~0.575 Ma Rockland ash bed (Fig. 6), suggesting a thickening of sediments southward from Hood. The <~0.211 to >~0.180 Ma dacitic ash of Hood, the youngest tephra identified in this study, occurs at a deeper depth in the more southern borehole B02 than the more northern borehole B25, recording a thickening of sediment packages into the central region of the delta. The varying sediment thicknesses can be used to calculate overall sediment accumulation rates using the depth and

https://doi.org/10.1016/j.yqres.2014.12.007 Published online by Cambridge University Press

approximate ages for each of the four tephra deposits identified in this study. Increasing sediment accumulation to the south suggests that variations in rates are related to differential subsidence as opposed to fluctuating sea level.

Approximate sediment accumulation rates from the Sacramento–San Joaquin Delta are calculated by dividing the sediment thickness (i.e., depth of tephra in boreholes; Table 1) by the tephrostratigraphic age. The oldest tephra and thinnest sediment thickness is encountered in the eastern region of the delta, where the ash of Wildcat Grade (<~1.450 to >~0.780 Ma) is sampled at ~60 m, resulting in an overall sediment accumulation rate ~0.04–0.08 m/1000 yr. Along a more central alignment, the Rockland ash bed (~0.575 Ma) is sampled at ~40 m depth, resulting in an overall sediment accumulation rate of ~0.07 m/1000 yr for the northern region of the delta. Rates are higher moving south along the central alignment. The Loleta ash bed (~0.390 Ma) is sampled at ~55 m depth, resulting in a sediment accumulation rate of ~0.14 m/1000 yr. The dacitic ash of Hood (<~0.211 to >~0.180 Ma) is sampled at ~39 m and ~53 m depth in the central region of the delta, resulting in rates ~0.18–0.22 m/1000 yr in the more northern sample and ~0.25–0.29 m/1000 yr in the more southern sample.

Overall, sediment accumulation rates are relatively low throughout the Sacramento–San Joaquin Delta. Gross estimates of accumulation rates are on the order of 0.07 m/1000 yr in the northern and eastern regions of the delta. Where sediments thicken in the central delta, rates may be as high as ~0.29 m/1000 yr. In comparison, high rates of sediment accumulation in major deltas are orders of magnitude higher than sediment accumulation rates in the Sacramento–San Joaquin Delta, although some rate variation may be due to comparison of differing time intervals (i.e., Sadler, 1981). For example, the late Quaternary Yangtze Delta (Chen et al., 2000 and references therein; Hori et al., 2001), the Ganges–Brahmaputra Delta (Goodbred and Kuehl, 2000) the Mississippi River Delta, U.S.A., (Corbett et al., 2006), the Mahakam Delta, Indonesia, (Roberts and Sydow, 1996, 2003; Storms et al., 2005), the Eastern Nile Delta, Egypt, (Coutellier and Stanley, 1987), the Red River Delta, Vietnam, (Hori et al., 2004), and the Yellow River Delta, North Yellow Sea, (Liu et al., 2004) can have Quaternary sediment accumulation rates up to two orders of magnitude higher than Quaternary rates calculated in the Sacramento–San Joaquin Delta. Sediment accumulation rates in fluvial systems, like those interpreted for tephra deposits in this study, vary by many orders of magnitude, and can be a record of rapid deposition in infrequent, climatically-driven events (e.g., Aalto et al., 2003). For example, Mississippi floodplains continue to accumulate sediment at higher rates than rates resulting from this study (e.g., Benedetti, 2003; Benedetti et al., 2007). Due to the large drainage area and associated large sediment supply that was likely funneled into the Quaternary Sacramento–San Joaquin Delta, accommodation space and tectonic influences on delta configuration likely limited accumulation.

Owing to the utility of tephra deposits as marker beds, tephra layers have been utilized in previous studies of fluvial-deltaic environments to constrain sedimentation rates (e.g., Peterson et al., 2012), but tephra are especially important markers in this study and other settings where shallowly-buried Quaternary sediments are too old for ^{14}C dating. Tephra are preserved in the Sacramento–San Joaquin Delta boreholes despite the low sediment accumulation rate. This suggests that other fluvial-deltaic settings in regions with known Quaternary volcanism may also contain buried tephra that would aid in complex subsurface chronostratigraphic correlations for future tectonic, climatic, and depositional studies. Where continuous core samples are unavailable, discontinuous geotechnical samples can provide necessary stratigraphic information and sample material to identify and correlate tephra.

Implications for hazard assessment and development in the Sacramento–San Joaquin Delta

Tephra ages, correlations, and associated variation in sediment accumulation rates throughout the Sacramento–San Joaquin Delta provide the basis for a Quaternary chronostratigraphic framework (Figs. 6 and 7). Such a framework is necessary for evaluating hazards related to tectonic deformation, liquefaction, and potential Quaternary activity of blind faults. Additionally, design and construction of a proposed water conveyance system through the Sacramento–San Joaquin Delta (i.e., California Department of Water Resources et al., 2013) and continued management of California's water and ecosystems resources require constraints on age and correlation of subsurface deposits in the study area. Results and interpretations from this study will serve as inputs for future stratigraphic modeling and hazard assessment related to infrastructure, resources, and populations that depend on the Sacramento–San Joaquin Delta.

Conclusions

Four distinct tephra are preserved in the Sacramento–San Joaquin Delta, identified in 27 boreholes, and correlated to regionally documented tephra with age constraints — the informally named ash of Wildcat Grade (<~1.450 to >~0.780 Ma), the Rockland ash bed (~0.575 Ma), the Loleta ash bed (~0.390 Ma), and the informally named dacitic ash of Hood (<~0.211 to >~0.180 Ma). Two of the tephra from the Sacramento–San Joaquin Delta boreholes, the Rockland ash bed and the Loleta ash bed, correlate to widespread tephra known throughout the western U.S. The Rockland ash bed is prevalent in deep (>40 m) boreholes in the northern region of the Sacramento–San Joaquin Delta, near Hood, and may be present in deeper deposits farther to the south that are not intersected by existing boreholes. The Rockland ash bed occurs as three facies in this study — 1) volcanic ash, and 2) pumice clasts interpreted to have been deposited in fluvial channel depositional environments, and 3) thin volcanic ash mixed with mud interpreted to represent overbank depositional environments. Due to the lack of volcanic sources in the study area and prevalent thick deposits of tephra Facies 1 and 2, the Rockland ash bed was likely concentrated in channels during a flood event following the volcanic eruption. The Loleta ash bed is identified in four boreholes in the northern region of the delta, south of Hood, and occurs as Facies 3, representative of deposition in overbank to floodplain environments from fluvial transport or reworked air-fall deposits. The informally named dacitic ash of Hood also occurs as thin Facies 3 deposits, but existing data does not allow facies interpretation for the informally named ash of Wildcat Grade.

Insights about tephra identification, correlation, and deposition provided by this study have implications for subsurface chronostragraphic correlations in the Sacramento–San Joaquin Delta, linkages to drainage basins and other regional deposits, and the utility of geotechnical borehole data and transported tephra deposits. The four tephra documented in this study give a broad, initial picture of depositional processes, varying sediment thicknesses, and accumulation rates within the Sacramento–San Joaquin Delta through time. Basal contacts of these tephra can be used as chronostratigraphic markers to correlate and constrain the ages of buried sediment packages. Characteristics of tephra in CDWR boreholes, and facies characterization will help to locate tephra in future boreholes intersecting geotechnically significant sediment packages below the modern Sacramento–San Joaquin Delta and help to define thickness variations in those packages. Insights provided by facies characterization of tephra deposits may be applicable to non-volcanic fluvial deposits in the study area.

Additionally, the approach and results discussed here are relevant to occurrences of tephra outside of the Sacramento–San Joaquin Delta. Other basins and depositional environments throughout the Pacific Northwest can now be linked to the delta's Pleistocene drainages and chronostratigraphic packages, particularly in locations with Rockland ash bed and Loleta ash bed deposits. In more distant global locations near Quaternary volcanism, examination of existing geotechnical

https://doi.org/10.1016/j.yqres.2014.12.007 Published online by Cambridge University Press

borehole data and new geotechnical sampling may reveal tephra layers useful for complex subsurface chronostratigraphic correlations. Even where tephra are reworked during fluvial transport, thick, concentrated deposits resulting from rapid deposition such as a flood event can provide crucial information.

Acknowledgments

Financial support for this research and the authors has been provided by the U.S. Geological Survey (USGS), California Department of Water Resources, the USGS Mendenhall Postdoctoral Fellowship (K.L. Maier), and the Delta Science Fellowship (E. Gatti). We thank Brad Aagaard, John Barron, Rob Barry, Mike Bennett, Tom Brocher, David Burtt, Matthew Coble, Steve DeLong, Shane Detweiler, Mike Diggles, Nick Hightower, Jack Hillhouse, Tom Holzer, Kristin Keenan, Keith Knudsen, Dave Perry, Carla Rosa, Scott Sochar, Steven Springhorn, Paul Spudich, Jorge Vasquez, Dave Wahl, and Heather Wright for supporting this research and manuscript development. We are grateful to Jon Warrick, Jason Addison, Siwan Davies, anonymous reviewers, Editor Kenneth Adams, and Senior Editor Derek Booth for providing thorough and helpful comments and reviews for this manuscript.

Appendix A. Supplementary data

Supplementary data to this article can be found online at http://dx.doi.org/10.1016/j.yqres.2014.12.007.

References

Addison, J.A., Beget, J.E., Ager, T.A., Finney, B.P., 2010. Marine tephrochronology of the Mt. Edgecumbe Volcanic Field, Southeast Alaska, USA. Quaternary Research 73, 277–292.

Aalto, R., Maurice-Bourgoin, L., Dunne, T., Montgomery, D.R., Nittrouer, C.A., Guyot, J.-L., 2003. Episodic sediment accumulation on Amazonian flood plains influenced by El Niño/Southern Oscillation. Nature 425, 493–497.

American Society for Testing and Materials, 2007. D2487 (2007) Standard Practice for Classification of Soils for Engineering Purposes (Unified Soil Classification System). ASTM International, West Conshohocken.

Atwater, B.F., 1982. Geologic maps of the Sacramento–San Joaquin Delta, California. U.S. Geological Survey MF-1401.

Barnard, P.L., Schoellhamer, D.H., Jaffe, B.E., McKee, L.J., 2013. Sediment transport in the San Francisco Bay Coastal System: an overview. Marine Geology 345, 3–17.

Bassinot, F.C., Labeyrie, L.D., Vincent, E., Quidelleur, X., Shackleton, N.J., Lancelot, Y., 1994. The astronomical theory of climate and the age of the Brunhes–Matuyama magnetic reversal. Earth and Planetary Science Letters 126, 91–108.

Benedetti, M.M., 2003. Controls on overbank deposition in the Upper Mississippi River. Geomorphology 56, 271–290.

Benedetti, M.M., Daniels, J.M., Ritchie, J.C., 2007. Predicting vertical accretion rates at an archaeological site on the Mississippi River floodplain: Effigy Mounds National Monument, Iowa. Catena 69, 134–149.

Brown, K.J., Pasternack, G.B., 2004. The geomorphic dynamics and environmental history of an upper deltaic floodplain tract in the Sacramento–San Joaquin Delta, California, USA. Earth Surface Processes and Landforms 29, 1235–1258.

Burton, C., Cutter, S.L., 2008. Levee failures and social vulnerability in the Sacramento–San Joaquin Delta Area California. Natural Hazards Review ASCE 136–149.

Byrne, R., Ingram, B.L., Starratt, S., Malamud-Roam, F., Collins, J.N., Conrad, M.E., 2001. Carbon-isotope, diatom, and pollen evidence for late Holocene salinity change in a brackish marsh in the San Francisco Estuary. Quaternary Research 55, 66–76.

California Department of Water Resources, U.S. Bureau of Reclamation, U.S. Fish Wildlife Service, National Marine Fisheries Service, 2013. Environmental Impact Report/Environmental Impact Statement for the Bay Delta Conservation International, Sacramento, CA. http://baydeltaconservationplan.com/Libraries/Dynamic_Document_Library/EIR-EIS_Title_Page_and_Table_of_Contents_5-10-13.sflb.ashx.

Chen, Z., Song, B., Wang, Z., Cai, Y., 2000. Late Quaternary evolution of the sub-aqueous Yangtze Delta, China: sedimentation, stratigraphy, palynology, and deformation. Marine Geology 162, 423–441.

Clifton, H.E., Leithold, E.L., 1991. Quaternary coastal and shallow-marine facies, northern California and the Pacific Northwest. In: Morrison, R.B. (Ed.), Quaternary Non-Glacial Geology: Conterminous United States. Decade of North American Geology Volume K-2. Geological Society of America, pp. 1156–1453.

Coutellier, V., Stanley, D.J., 1987. Late Quaternary stratigraphy and paleogeography of the eastern Nile Delta, Egypt. Marine Geology 77, 257–275.

Coons, T., Soulard, C.E., Knowles, N., 2008. High-resolution digital terrain models of the Sacramento/San Joaquin Delta region, California. U.S. Geological Survey Data Series 359.

Corbett, D.R., McKee, B., Allison, M., 2006. Nature of decadal-scale sediment accumulation on the western shelf of the Mississippi River delta. Continental Shelf Research 26, 2125–2140.

Dettinger, M.D., Ingram, B.L., 2013. The coming megafloods. Scientific American 308, 64–71.

Deverel, S.J., Rojstaczer, S., 1996. Subsidence of agricultural lands in the Sacramento–San Joaquin Delta, California: role of aqueous and gaseous carbon fluxes. Water Resources Research 32, 2359–2367.

Donnelly-Nolan, J.M., 2010. Geologic map of Medicine Lake volcano, northern California. U.S. Geological Survey Scientific Investigations Map 2927 (48 pp., 2 sheets).

Donnelly-Nolan, J.M., Champion, D.E., Lanphere, M.A., Ramsey, D.W., 2004. New thoughts about Newberry Volcano, central Oregon, USA. Eos, Transactions of the American Geophysical Union 85 (abs. V43E-1452).

Drexler, J.Z., de Fountaine, C.S., Knifong, D.L., 2007. Age determination of the remaining peat in the Sacramento–San Joaquin Delta, California, USA. U.S. Geological Survey Open-File Report 2007-1303 (2 pp., http://pubs.usgs.gov/of/2007/1303/).

Drexler, J.Z., de Fontaine, C.S., Brown, T.A., 2009. Peat accretion histories during the past 6,000 years in marshes in the Sacramento–San Joaquin Delta, California, USA. Estuaries and Coasts 32, 871–892.

Drexler, J.Z., Paces, J.B., Alpers, C.N., Windham-Myers, L., Neymark, L.A., Bullen, T.D., Taylor, H.E., 2014. $^{234}U/^{238}U$ and $\delta^{87}Sr$ in peat as tracers of paleosalinity in the Sacramento–San Joaquin Delta of California, USA. Applied Geochemistry 40, 164–179.

Finch, M.O., 1988. Estimated performance of Twitchell Island levee system, Sacramento–San Joaquin Delta, under maximum credible earthquake conditions. Bulletin of the Association of Engineering Geologists AEGBBU 25, 207–217.

Gatti, E., Durant, A.J., Gibbard, P.L., Oppenheimer, C., 2011. Youngest Toba Tuff in the Son Valley, India: a weak and discontinuous stratigraphic marker. Quaternary Science Reviews 30, 3925–3934.

Gatti, E., Mokhtar, S., Talib, K., Rashidi, N., Gibbard, P., Oppenheimer, C., 2013. Depositional processes of reworked tephra from the Late Pleistocene Youngest Toba Tuff deposits in the Lenggong Valley, Malaysia. Quaternary Research 79, 228–241.

Goman, M., Wells, L., 2000. Trends in river flow affecting the northeastern reach of the San Francisco Bay Estuary over the past 7000 years. Quaternary Research 54, 206–217.

Goodbred Jr., S.L., Kuehl, S.A., 2000. The significance of large sediment supply, active tectonism, and eustasy on margin sequence development: Late Quaternary stratigraphy and evolution of the Ganges–Brahmaputra delta. Sedimentary Geology 133, 227–248.

Grabau, A.W., 1913. Principles of Stratigraphy. A.G. Seiler and Co., New York.

Graymer, R.W., Jones, D.L., Brabb, E.E., 2002. Geologic map and database of northeastern San Francisco Bay region, California: U.S. Geological Survey Miscellaneous Field Studies Mapp MF-2403, scale 1:100,000.

Herrero-Bervera, E., Helsley, C.E., Sarna-Wojcicki, A.M., Lajoie, K.R., Meyer, C.E., McWilliams, M.O., Negrini, R.M., Turrin, B.D., Donnelly-Nolan, J.M., Liddicoat, J.C., 1994. Age and correlation of a paleomagnetic episode in the western United States by $^{40}Ar/^{39}Ar$ dating and tephrochronology: The Jamaica, Blake, or a new polarity episode? Journal of Geophysical Research 99, 24,091–24,103.

Hori, K., Saito, Y., Zhao, Q., Cheng, X., Wang, P., Sato, Y., Li, C., 2001. Sedimentary facies and Holocene progradation rates of the Changjiang (Yangtze) delta, China. Geomorphology 41, 233–248.

Hori, K., Tanabe, S., Saito, Y., Haruyama, S., Nguyen, V., Kitamura, A., 2004. Delta initiation and Holocene sea-level change: example from the Song Hong (Red River) delta, Vietnam. Sedimentary Geology 164, 237–249.

Ingebritsen, S.E., Ikehara, M.E., Galloway, D.L., Jones, D.R., 2000. Delta subsidence in California: the sinking heart of the State. U.S. Geological Survey Fact Sheet 005-00 (4 pp., http://pubs.usgs.gov/fs/2000/fs00500/).

Ingram, B.L., Ingle, J.C., Conrad, M.E., 1996. A 2000 yr record of Sacramento–San Joaquin river inflow to San Francisco Bay estuary, California. Geology 24, 331–334.

Jackson, W.T., Paterson, A.M., 1977. The Sacramento–San Joaquin Delta: the evolution and implementation of water policy: an historical perspective. Technical Completion Report. California Water Resources Center, University of California, Davis, Davis, California, pp. 1–185.

Jassby, A.D., Cloern, J.E., 2000. Organic matter sources and rehabilitation of the Sacramento–San Joaquin Delta (California, USA). Aquatic Conservation: Marine and Freshwater Ecosystems 10, 323–352.

Kataoka, K., Nakajo, T., 2002. Volcaniclastic resedimentation in distal fluvial basins induced by large-volume explosive volcanism: the Ebisutoge–Fukuda tephra, Plio-Pleistocene boundary, central Japan. Sedimentology 49, 319–334.

Kataoka, K., 2005. Distal fluvio-lacustrine volcaniclastic resedimentation in response to an explosive silicic eruption: the Pliocene Mushono tephra bed, central Japan. Geological Society of America Bulletin 117, 3–17.

Kataoka, K.S., Manville, V., Nakajo, T., Urabe, A., 2009. Impacts of explosive volcanism on distal alluvial sedimentation: examples from the Pliocene–Holocene volcaniclastic successions of Japan. Sedimentary Geology 220, 306–317.

Königer, S., Stollhofen, H., 2009. Environmental and Tectonic Controls on Preservation Potential of Distal Fallout Ashes in Fluvio-Lacustrine Settings: The Carboniferous–Permina Saar–Nahe Basin, South-West Germany. Volcaniclastic Sedimentation in Lacustrine Settings, Special Publication 30 of the International Association of Sedimentologists 15 (263 pp.).

Krug, E.H., Cherven, V.B., Hatten, C.W., Roth, J.C., 1992. Subsurface structure in the Montezuma Hills, southwestern Sacramento Basin. In: Cherven, V.B., Edmonson, W.F. (Eds.), Structural geology of the Sacramento Basin. American Association of Petroleum Geologists, Pacific Section Miscellaneous Publication 41, pp. 41–60.

Lanphere, M.A., Champion, D.E., Clynne, M.A., Lowenstern, J.B., Sarna-Wojcicki, A.M., Wooden, J.L., 2004. Age of the Rockland tephra, western USA. Quaternary Research 62, 94–104.

Leahy, K., 1997. Discrimination of reworked pyroclastics from primary tephra-fall tuffs: a case study using kimberlites of Fort a la Corne, Saskatchewan, Canada. Bulletin of Volcanology 59, 65–71.
Le Bas, M.J., Lemaitre, R.W., Streckeisen, A., Zanettin, B., 1986. A chemical classification of volcanic rocks based on the total alkali silica diagram. Journal of Petrology 27, 745–750.
Lettis, W.R., 1982. Late Cenozoic stratigraphy and structure of the western margin of the Central San Joaquin Valley, California. U.S. Geological Survey Open File Report 82-526 (203 pp., http://pubs.usgs.gov/of/1982/0526/).
Liu, J.P., Milliman, J.D., Gao, S., Cheng, P., 2004. Holocene development of the Yellow River's subaqueous delta, North Yellow Sea. Marine Geology 209, 45–67.
Logan, S.H., 1990. Global warming and the Sacramento–San Joaquin Delta. California Agriculture 44, 16–18.
Lowe, D.J., 2008. Globalization of tephrochronology: new views from Australasia. Progress in Physical Geography 32, 311–335.
Lowe, D.J., 2011. Tephrochronology and its application: a review. Quaternary Geochronology 6, 107–153.
Lowe, D.R., 1988. Suspended-load fallout rate as an independent variable in the analysis of current structures. Sedimentology 35, 765–776.
Luedke, R.G., Smith, R.L., 1991. Quaternary volcanism in the western conterminous United States. In: Morrison, R.B. (Ed.), Quaternary Non-glacial Geology: Conterminous United States. Decade of North American Geology Volume K-2. Geological Society of America, pp. 75–92.
Mack, G.H., McIntosh, W.C., Leeder, M.R., Monger, H.C., 1996. Plio-Pleistocene pumice floods in the ancestral Rio Grande, southern Rio Grande rift, USA. Sedimentary Geology 103, 1–8.
Maier, K.L., Ponti, D.J., Tinsley, J.C., Gatti, E., Pagenkopp, M., 2014. Geologic logs of geotechnical cores from the subsurface Sacramento–San Joaquin Delta, California. U.S. Geological Survey Open-File Report 2014-1127 http://dx.doi.org/10.3133/ofr20141127 (16 pp.).
Malamud-Roam, F.P., Ingram, B.L., Hughes, M., Florsheim, J.L., 2006. Holocene paleoclimate records from a large California estuarine system and its watershed region: linking watershed climate and bay conditions. Quaternary Science Reviews 25, 1570–1598.
Manville, V., Newton, E.H., White, J.D.L., 2005. Fluvial responses to volcanism: resedimentation of the 1800a Taupo ignimbrite eruption in the Rangitaiki River catchment, North Island, New Zealand. Geomorphology 65, 49–70.
Manville, V., Németh, K., Kano, K., 2009. Source to sink: a review of three decades of progress in the understanding of volcaniclastic processes, deposits, and hazards. Sedimentary Geology 220, 136–161.
McGann, M., Erikson, L., Wan, E., Powell, C., Maddocks, R.F., 2013. Distribution of biologic, anthropogenic, and volcanic constituents as a proxy for sediment transport in the San Francisco Bay Coastal System. Marine Geology 345, 113–142.
Miall, A.D., 1977a. Fluvial sedimentology: a historical review. Canadian Society of Petroleum Geologists Memoir 5, 1–47.
Miall, A.D., 1977b. Lithofacies types and vertical profile models in braided river deposits: a summary. Canadian Society of Petroleum Geologists Memoir 5, 597–604.
Mount, J., Twiss, R., 2005. Subsidence, sea level rise, and seismicity in the Sacramento–San Joaquin Delta. San Francisco Estuary & Watershed Science 3, 1–18.
Murray-Wallace, C.V., Woodroffe, C.D., 2014. Quaternary Sea-level Changes: A Global Perspective. Cambridge University Press.
Nakayama, K., Yoshikawa, S., 1997. Depositional processes of primary to reworked volcaniclastics on an alluvial plain: an example from the Lower Pliocene Ohta tephra bed of the Tokai Group, central Japan. Sedimentary Geology 107, 211–229.
Nooren, C.A.M., Hoek, W.Z., Tebbens, L.A., Martin Del Pozzo, A.L., 2009. Tephrochronological evidence for the late Holocene eruption history of El Chichón Volcano, Mexico. Geofísica Internacional 48, 97–112.
Ogle, B.A., 1953. Geology of the Eel River Valley area, Humboldt County, California. California Division of Mines Bulletin 164, 128.
Peterson, C., Minor, R., Gates, E.B., Vanderburgh, S., Carlisle, K., 2012. Correlation of tephra marker beds in the latest Pleistocene and Holocene fill of the submerged Lower Columbia River Valley, Washington and Oregon, U.S.A. Journal of Coastal Research 28, 1362–1380.
Postma, G., 1983. Water escape structures in the context of a depositional model of a mass flow dominated conglomeratic fan-delta (Abrioja Formation, Pliocene, Almeria Basin, SE Spain). Sedimentology 30, 91–103.
Pouget, S., Bursik, M., Cortés, J.A., Hayward, C., 2014. Use of principal component analysis for identification of Rockland and Trego Hot Springs tephra in the Hat Creek Graben, northeastern California, USA. Quaternary Research 81, 125–137.
Real, C.R., Knudsen, K.L., 2009. Collaborative research with URS, Corporation, California Geological Survey: application of new liquefaction hazard mapping techniques to the Sacramento–San Joaquin Delta area. Final Technical Report, pp. 1–56.
Real, C.R., Knudsen, K.L., Woods, M.O., 2010. Application of new liquefaction hazard mapping techniques to the Sacramento–San Joaquin Delta. American Geophysical Union Fall Meeting 2010 (Abstract #NH11A-1106).
Roberts, H.H., Sydow, J., 1996. The offshore Mahakam delta: stratigraphic response of late Pleistocene-to-modern sea level cycle. Proceedings Indonesian Petroleum Association 25, pp. 147–161.
Roberts, H.H., Sydow, J., 2003. Late Quaternary stratigraphy and sedimentology of the offshore Mahakam delta, East Kalimantan (Indonesia). In: Sidi, F.H., Nummendal, D., Imbert, P., Darman, H., Posamentier, H.W. (Eds.), Tropical Deltas of Southeast Asia; Sedimentology, Stratigraphy, and Petroleum Geology. SEPM Special Publication 76, pp. 125–145.
Sadler, P.M., 1981. Sediment accumulation rates and the completeness of stratigraphic sections. Journal of Geology 89, 569–584.
Salisbury, M.J., Patton, J.R., Kent, A.J.R., Goldfinger, C., Djadjadihardja, Y., Hanifa, U., 2012. Deep-sea ash layers reveal evidence for large, late Pleistocene and Holocene explosive activity from Sumatra, Indonesia. Journal of Volcanology and Geothermal Research 231–232, 61–71.
Sarna-Wojcicki, A.M., 1976. Correlation of late Cenozoic tuffs in the central Coast Ranges of California by means of trace- and minor-element chemistry. U.S. Geological Survey Professional Paper 972 (32 pp.).
Sarna-Wojcicki, A.M., 2000. Tephrochronology. In: Noller, J.S., Sowers, J.M., Lettis, W.R. (Eds.), Quaternary Geochronology: Methods and Applications. American Geophysical Union, Washington, DC, pp. 357–378.
Sarna-Wojcicki, A.M., Bowman, H.R., Russell, P.C., 1979. Chemical correlation of same late Cenozoic tuffs of northern and central California by neutron-activation analysis of glass and comparison with X-ray fluorescence analysis. U.S. Geological Survey Professional Paper 1147 (15 pp.).
Sarna-Wojcicki, A.M., Bowman, H.R., Meyer, C.E., Russell, P.C., Woodward, M.J., McCoy, G., Rowe Jr., J.J., Baedecker, P.A., Asaro, F., Michael, H., 1984. Chemical analyses, correlations, and ages of Pliocene and Pleistocene ash layers of east-central and southern California. U.S. Geological Survey Professional Paper 1293 (41 pp.).
Sarna-Wojcicki, A.M., Davis, J.O., 1991. Quaternary tephrochronology. In: Morrison, R.B. (Ed.), Geological Society of America, pp. 93–116.
Sarna-Wojcicki, A.M., Lajoie, K.R., Meyer, C.E., Adam, D.P., Rieck, H.J., 1991. Tephrochronologic correlation of upper Neogene sediments along the Pacific margin, conterminous United States. In: Morrison, R.B. (Ed.), Quaternary Non-glacial Geology: Conterminous United States. Decade of North American Geology volume K-2. Geological Society of America, pp. 117–140.
Sarna-Wojcicki, A.M., Meyer, C.E., Bowman, H.R., Hall, N.T., Russell, P.C., Woodward, M.J., Slate, J.L., 1985. Correlation of the Rockland ash bed, a 400,000-year-old stratigraphic marker in northern California and western Nevada, and implications for Middle Pleistocene paleogeography of central California. Quaternary Research 23, 236–257.
Sarna-Wojcicki, A.M., Meyer, C.E., Nakata, J.K., Scott, W.E., Russell, P.C., 1989. Age and correlation of mid-Quaternary ash beds and tuffs in the vicinity of Bend, Oregon. In: Scott, W.E., Gardner, C.A., Sarna-Wojcicki, A.M. (Eds.), Guidebook for Field Trip to the Mount Bachelor-South Sister-Bend Area, Central Oregon High Cascades. U.S. Geological Survey, pp. 55–62.
Sarna-Wojcicki, A.M., Morrison, S.D., Meyer, C.E., Hillhouse, J.W., 1987. Correlation of upper Cenozoic tephra layers between sediments of the western United States and eastern Pacific Ocean and comparison with biostratigraphic and magnetostratigraphic age data. Geological Society of America Bulletin 98, 207–223.
Shane, P.A.R., 1991. Remobilized silicic tuffs in middle Pleistocene fluvial sediments, southern North Island, New Zealand. New Zealand Journal of Geology and Geophysics 34, 489–499.
Singer, B.S., Jicha, B.R., Kirby, B.T., Geissman, J.W., Herrero-Bervera, E., 2008. $^{40}Ar/^{39}Ar$ dating links Albuquerque volcanoes to Pringle Falls excursion and the geomagnetic instability time scale. Earth and Planetary Science Letters 267, 584–595.
Starratt, S.W., 2002. Diatoms as indicators of freshwater flow variation in central California. In: West, G.J., Buffaloe, L.D. (Eds.), Proceedings of the Eighteenth Annual Pacific Climate Workshop, Technical Report 68 of the Interagency Ecological Program for the San Francisco Estuary, pp. 129–144.
Starratt, S.W., 2004. Diatoms as indicators of late Holocene freshwater flow variations in the San Francisco Bay estuary, Central California, USA. Proceedings of the Seventeenth International Diatom Symposium, pp. 371–397.
Storms, J.E.A., Hoogendoorn, R.M., Dam, R.A.C., Hoitink, A.J.F., Kroonenberg, S.B., 2005. Late-Holocene evolution of the Mahakam delta, East Kalimantan, Indonesia. Sedimentary Geology 180, 149–166.
Taylor, E.M., 1981. Central high Cascade roadside geology, Bend, Sisters, McKenzie Pass, and Santiam Pass, Oregon. U.S. Geological Survey Circular 838, 55–58.
Tripaldi, A., Zárate, M.A., Brook, G.A., Li, G.-Q., 2011. Late Quaternary paleoenvironments and paleoclimatic conditions in the distal Andean piedmont, southern Mendoza, Argentina. Quaternary Research 76, 253–263.
Unruh, J.R., Hitchcock, C.S., Hector, S., Blake, K., 2009. Characterization of Potential Seismic Sources in the Sacramento–San Joaquin Delta, California, Final Technical Report. U.S. Geological Survey, National Earthquake Hazards Reduction Programpp. 1–45.
Unruh, J.R., Krug, K., 2007. Assessment and Documentation of Transpressional Structures, Northeastern Diablo Range, for the Quaternary Fault Map Database: Collaborative Research with William Lettis & Associates, Inc., and the U.S. Geological Survey: Final Technical Report, Priority III: Construction of a Community Quaternary Fault Database. U.S. Geological Survey, National Earthquake Hazards Reduction Program, pp. 1–45.
Wan, E., 1988. Late Neogene planktonic foraminiferal biostratigraphy of Deep-Sea Drilling Project Leg 5, Site 36: Northeast Pacific Ocean. Unpublished Master's thesis, University of California, Berkeley, Berkeley, California, 129 pp.
Williams, R.M.E., Grotzinger, J.P., Dietrich, W.E., Gupta, S., Sumner, D.Y., Wiens, R.C., Mangold, N., Malin, M.C., Edgett, K.S., Maurice, S., Forni, O., Gasnault, O., Ollila, A., Newsom, H.E., Dromart, G., Palucis, M.C., Yingst, R.A., Anderson, R.B., Herkenhoff, K.E., Le Mouélic, S., Goetz, W., Madsen, M.B., Koefoed, A., Jensen, J.K., Bridges, J.C., Schwenzer, S.P., Lewis, K.W., Stack, K.M., Rubin, D., Kah, L.C., Bell III, J.F., Farmer, J.D., Sullivan, R., Van Beek, T., Blaney, D.L., Pariser, O., Deen, R.G., M.S.L. Science Team, 2013. Martian fluvial conglomerates at Gale Crater. Science 340, 1068–1072.
Wong, I., Coppersmith, K., Yongs, B., McGann, M., 2006. Probabilistic seismic hazard analysis for ground shaking and estimation of earthquake scenario probabilities. Delta Risk Management Strategy, Initial Technical Framework Paper (10 pp.).
Woodward Clyde Consultants, 1980. Evaluation of the potential for resolving the geologic and seismic issues in Humboldt Bay Power Plant Unit Number 3. Unpublished consulting report prepared for Pacific Gas and Electric Company, Appendices A, B and C.
Wright, S.A., Schoellhamer, D.H., 2005. Estimating sediment budgets at the interface between rivers and estuaries with application to the Sacramento–San Joaquin River Delta. Water Resources Research 41, 1–17.
Yu, E., Segall, P., 1996. Slip in the 1868 Hayward earthquake from the analysis of historical triangulation data. Journal of Geophysical Research 101, 16,101–116,118.